

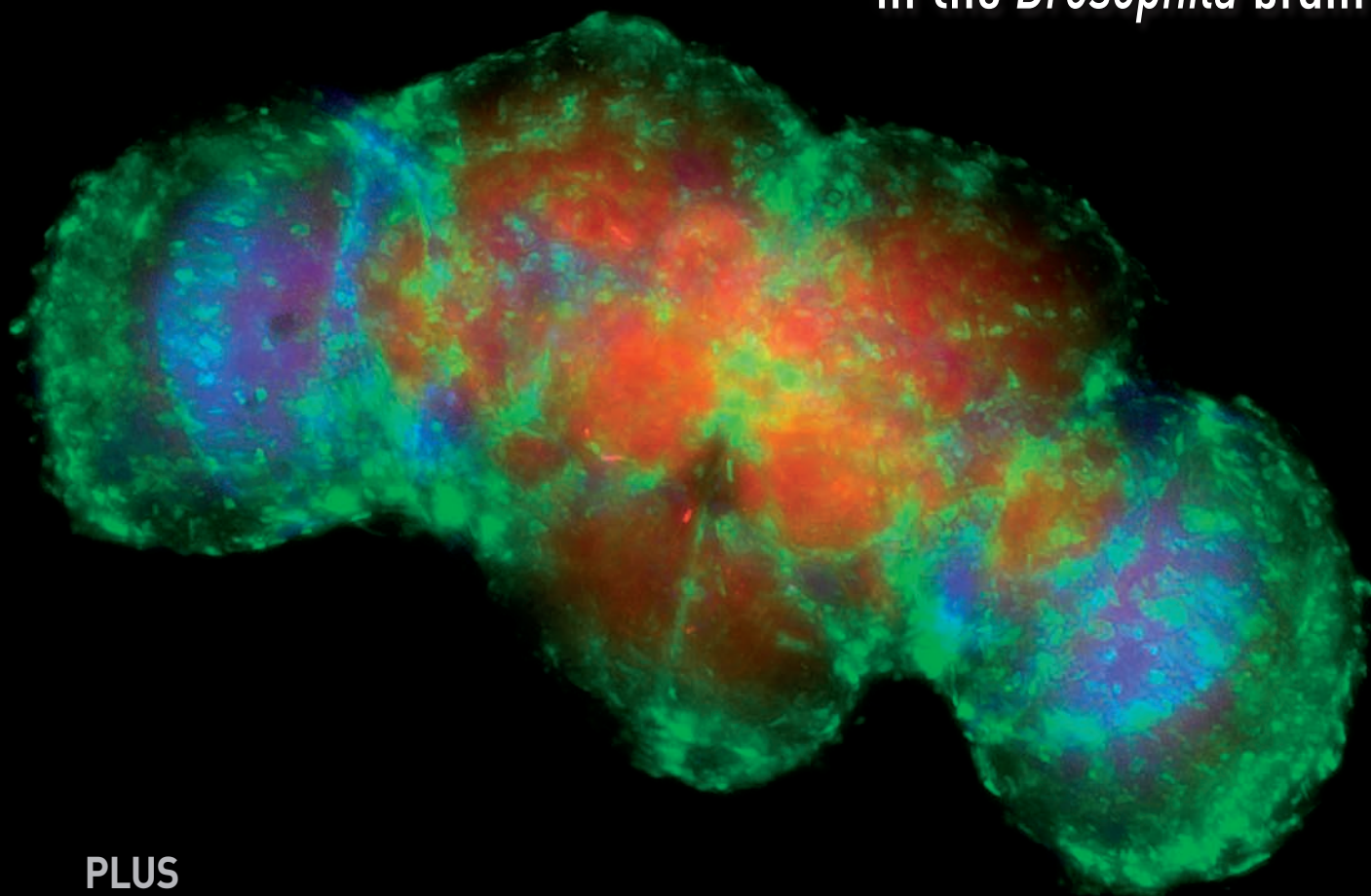
JUNE 2015

BIOPROBES 71

MOLECULAR PROBES™ JOURNAL OF CELL BIOLOGY APPLICATIONS

SPECIAL FLOW CYTOMETRY ISSUE

A sensitive flow cytometry assay
for hyperploidy and cell death
in the *Drosophila* brain



PLUS

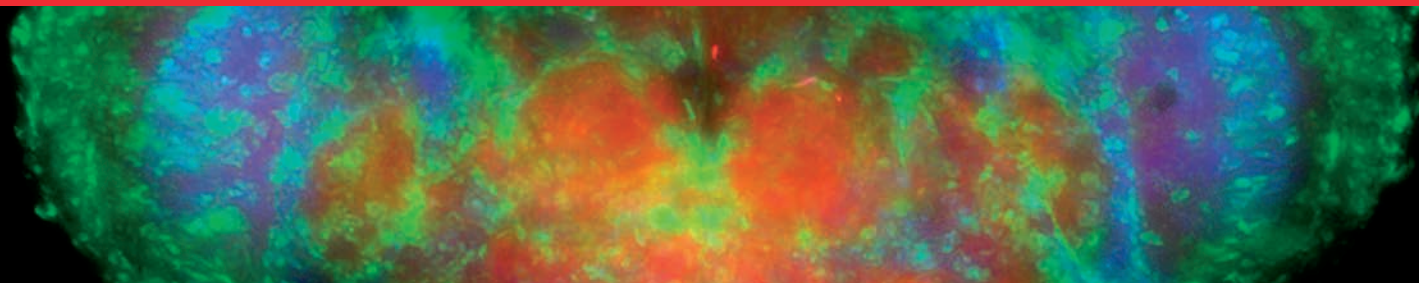
Flow cytometry panel design

Tools and strategies for rare-event detection

Multiparameter detection of early apoptosis markers

Instrument specifications for the Attune™ NxT cytometer

invitrogen
by Thermo Fisher Scientific



Production Manager

Beth Browne

Senior Editor

Michelle Spence

Designer

Lynn Soderberg

Editors

Sarah Adai
Tom Landon
Grace Richter

Contributors

Brian Almond
Trillium Blackmer
Veronica Blackston
Jolene Bradford
Beth Browne
Suzanne Buck
Laura Buttitta¹
Daniel Cash
Kevin Chambers
Andrea Cossarizza²
Sara De Biasi²
Carmen Finnissy
Helen Fleisig
Kathleen Free
Lara Gibellini²
Olga Grushko¹
Kamran Jamil
Greg Kaduchak
Bente Kierulf
Anette Kullmann
Ryan Larson
Mu Li
Bhaskar Mandavilli
Penny Melquist
Axl Neurauter
Morten Oksvold^{3,4}
Shane Oram
Paola Paglia
Ketil Pedersen
Natasha Roark
Norbert Roos⁴
Barbara Seredick
Alexander Vlassov

¹ University of Michigan, United States

² University of Modena and Reggio Emilia, Italy

³ Oslo University Hospital, Norway

⁴ University of Oslo, Norway

ONLINE AND ON THE MOVE

- 2 | Updated Molecular Probes™ apps, *Flow Cytometry Products and Resource Guide*, and more

JUST RELEASED

- 4 | Our newest cellular analysis products and technologies

CURRENT RESEARCH

- 6 | A sensitive assay for hyperploidy and cell death in the *Drosophila* brain using the Attune™ Acoustic Focusing Cytometer
10 | Isolation and characterization of exosomes using magnetic beads

LITERATURE REVIEW

- 14 | Few and far between
Tools and strategies for rare-event detection using flow cytometry

PRACTICAL APPLICATIONS

- 19 | The next generation in acoustic focusing cytometry
The Attune™ NxT Acoustic Focusing Cytometer
20 | Flow cytometry panel design: The basics
Multiplex flow cytometry experiments need the right combination of fluorophores
23 | Keep pace with the surge in fluorescent protein choices
Multicolor detection of fluorescent protein expression with the Attune™ NxT Acoustic Focusing Cytometer
26 | Minimize—even eliminate—color compensation
No-compensation immunophenotyping using a four-laser flow cytometer
28 | First, do no harm
No-lyse, no-wash assays for the Attune™ NxT Acoustic Focusing Cytometer

JOURNAL CLUB

- 31 | Multiparameter detection of early apoptosis markers without compensation
Uncompensated polychromatic analysis of mitochondrial membrane potential using JC-1 and multilaser excitation

Published by Thermo Fisher Scientific Inc. © 2015

BioProbes™ Journal, available in print and online at thermofisher.com/bioprobates, is dedicated to providing researchers with the very latest information about cell biology products and their applications. For a complete list of our products, along with extensive descriptions and literature references, please see our website.

Subscribe to *BioProbes™ Journal* at thermofisher.com/subscribebp

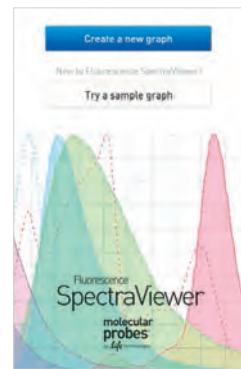


SpectraViewer mobile app: Now compatible with Android™ and iPhone™ devices

The Molecular Probes™ Fluorescence SpectraViewer mobile app is now available for Android™ phones, and we have updated our iPhone™ and iPad™ version to be compatible with iOS™ 8. This mobile SpectraViewer acts as an extension of our online Fluorescence SpectraViewer, in which you can:

- View and compare the spectra of fluorescent dyes and proteins
- Add unlimited emission and excitation filters per plot
- Email plots and configurations to yourself or your colleagues in a clear, printable format

With a mobile-friendly display and user interface, the SpectraViewer app allows you to search an extensive list of fluorophores and check spectral compatibility when at your lab bench or while you are out and about. Download this mobile app at the App Store™ for iPhone™ and iPad™ devices or at Google Play™ for Android™ phones and tablets, and see our complete selection of mobile and desktop apps at thermofisher.com/apps.

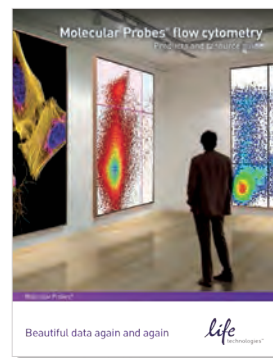


Molecular Probes™ Flow Cytometry Products and Resource Guide

The Molecular Probes™ Flow Cytometry Products and Resource Guide provides an overview of the products and techniques used in flow cytometry workflows, including:

- Sample preparation—from cell preservation to cell isolation
- Instrument setup and calibration—from alignment to absolute cell counting
- Antigen detection—from primary antibodies to custom services
- Cell analysis—from cell health and viability to phagocytosis

Request your copy today—in print or digital format—at thermofisher.com/flowguide.



PubGo™ plugin: Enhance your publication reading

The PubGo™ plugin (beta version) for use with Adobe™ Reader™ and Adobe™ Acrobat™ software is designed to complement your publication-reading experience by providing additional information about products that are mentioned in a PDF. The first time you download the plugin, you will be asked to associate it with your active version of Adobe™ software. Then each time you open a PDF, the tool will automatically run in the background, identifying related products where appropriate and providing additional information for selected Thermo Fisher Scientific products. With this plugin, you can:

- Quickly identify relevant products and related information (e.g., product protocols, prices, alternate sizes)
- Easily find replacement products when reading an older article citing a product that is no longer available
- Access direct links to more detailed product information

The PubGo™ plugin is available for both Windows™ and Mac OS™ operating systems. Download it today at thermofisher.com/pubgo.

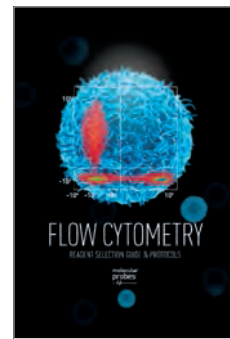


Molecular Probes™ flow cytometry mobile app: Protocols at your fingertips

The Molecular Probes™ Flow Cytometry Reagent Guide and Protocols mobile app is designed to help you find fluorescent reagents, kits, and flow cytometry protocols for your cell biology research. Also included are product guides for instrument calibration and setup, protein labeling, and secondary detection. Key features of the app include:

- Straightforward experimental design, with excitation and emission data for every reagent
- Quick and easy protocols, with a built-in protocol timer that runs even if you leave the app
- Examples of data output for every product

Download this mobile app at the App Store™ for iPhone™ and iPad™ devices or at Google Play™ for Android™ phones and tablets, and see our complete selection of mobile and desktop apps at thermofisher.com/apps.

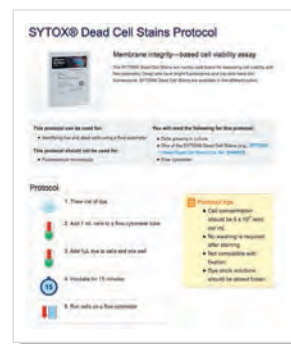


Online cell analysis protocols: Now searchable and sortable

The new “Cell Analysis Protocols” page organizes our staining protocols by platform: flow cytometry, high-content analysis, imaging, and microplate assays; and by application: cell viability, cell proliferation, and cell structure. Simply select the arrow at the top of the column to sort the table for your convenience, or search for the fluorescent probe you are interested in. You’ll find protocols for:

- Cell viability assays with LIVE/DEAD™ reagents
- Cell proliferation assays with CellTrace™ reagents
- Nucleic acid staining with SYTO™ and SYTOX™ dyes

And more! Visit the protocols page today at thermofisher.com/ca-protocols.

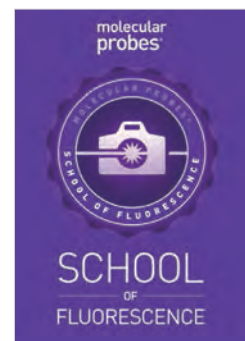


Molecular Probes™ School of Fluorescence

Learn the fundamentals of fluorescence imaging from Molecular Probes scientists. We’ve spent hundreds of hours in the lab and want to share our best tips, tricks, and protocols for capturing beautiful images, including:

- Fundamentals of fluorescence microscopy
- Sample and fluorescent label considerations
- Capturing and analyzing your labeled samples
- Live- and fixed-cell staining protocols

It’s our aim to include everything that we wish we had known when we started working with fluorescent imaging reagents, and we asked our Technical Support team to review each section to make sure we haven’t overlooked anything. Even though we can’t be right there in the lab with you when you do your experiments, we hope you’ll benefit from the information we’ve collected. See for yourself at thermofisher.com/mpsf.

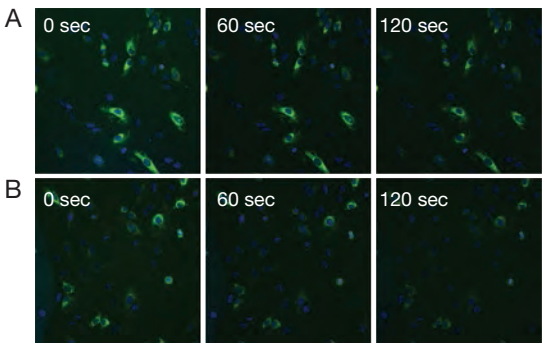


ProLong™ Live Antifade Reagent: Minimize photobleaching in live cells

ProLong™ Live Antifade Reagent helps reduce the loss of fluorescence that occurs with photobleaching during live-cell imaging. When illuminated, fluorescent dyes can degrade, reducing fluorescence intensity and leading to the creation of singlet oxygen (¹O₂), a highly reactive excited state of oxygen that can further degrade neighboring dye molecules. ProLong™ Live Antifade Reagent metabolizes ¹O₂, helping to maintain the intensity and duration of sample fluorescence. Moreover, we have observed little to no effect of ProLong™ Live reagent on cell viability and proliferation in experiments lasting up to 48 hours. Benefits of ProLong™ Live Antifade Reagent include:

- Reduced photobleaching in live-cell experiments with fluorophores and fluorescent proteins across the spectrum
- Extended imaging times in time-lapse experiments
- Ease of use—just add to the imaging solution, complete cell culture medium, or buffer, and then incubate and image

See thermofisher.com/antifades for more information on ProLong™ Live reagent, as well as the full line of Molecular Probes™ antifade reagents.



Photobleaching protection by ProLong™ Live Antifade Reagent in live cells. HeLa cells were transduced with CellLight™ Mitochondria-GFP for 24 hr, then labeled with Hoechst™ 33342 for 15 min. Samples incubated with ProLong™ Live Antifade Reagent for 2 hr retained more signal at all time points **(A)**, when compared with control samples in complete medium alone **(B)**.

Product	Quantity	Cat. No.
ProLong™ Live Antifade Reagent	5 x 1 mL	P36974
	1 mL	P36975

Foxp3 Transcription Factor Staining Buffer Kits

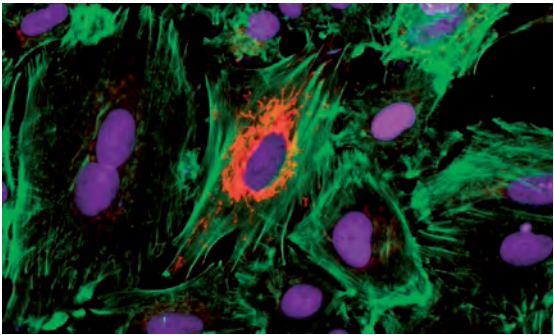
The Foxp3 Transcription Factor Staining Buffer Kits provide the fixation and permeabilization buffers needed for easy detection of intracellular Foxp3 transcription factor using fluorescent antibody conjugates. The buffer systems are available with either APC-, FITC-, or PE-conjugated anti-mouse Foxp3 monoclonal antibody (clone 3G3); staining buffers are also available separately (see thermofisher.com/foxp3buffer).

Foxp3 Transcription Factor Staining Buffer Kit	Quantity	Cat. No.
Staining Buffer Kit (compatible with Foxp3 mAb)	1 kit	A25866A
With Foxp3 Mouse Anti-Mouse mAb (clone 3G3), APC conjugate	1 kit	A25863A
With Foxp3 Mouse Anti-Mouse mAb (clone 3G3), FITC conjugate	1 kit	A25864A
With Foxp3 Mouse Anti-Mouse mAb (clone 3G3), PE conjugate	1 kit	A25865A

Multiplexable Click-iT™ Plus TUNEL Assay for *in situ* detection of apoptosis

The Click-iT™ Plus TUNEL Assay detects apoptotic cells in tissues and cultured cells through the use of a small, highly specific labeling moiety and a brightly fluorescent dye. Once the alkyne-modified dUTP is incorporated into DNA fragments, detection is achieved with an Alexa Fluor™ azide through a catalyzed “click” reaction using conditions mild enough to preserve the fluorescent signal from GFP or RFP. The Click-iT™ Plus TUNEL Assay has been validated with several different formalin-fixed, paraffin-embedded tissue types; in all cases, the ability to multiplex with fluorescent proteins and dyes was preserved. Learn more at thermofisher.com/clickit-tunel.

Click-iT™ Plus TUNEL Assay for <i>In Situ</i> Apoptosis	Quantity	Cat. No.
With Alexa Fluor™ 488 dye	1 kit	C10617
With Alexa Fluor™ 594 dye	1 kit	C10618
With Alexa Fluor™ 647 dye	1 kit	C10619

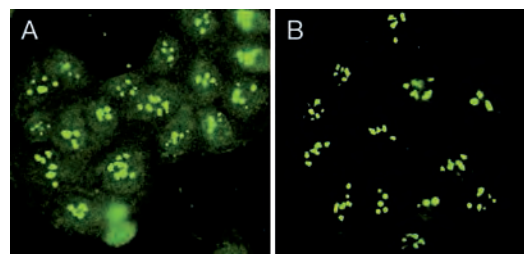


Multiplexing with the Click-iT™ Plus TUNEL Assay. HeLa cells transduced with CellLight™ Mitochondria-RFP, BacMam 2.0 and treated with DNase to induce DNA strand breaks were analyzed using the Click-iT™ Plus TUNEL Assay (with Alexa Fluor™ 647 dye) to detect fragmented DNA (purple). ActinGreen™ 488 ReadyProbes™ Reagent was used to label actin filaments (green), and RFP expression was localized to mitochondria (red).

Superclonal™ secondary antibodies: Minimize cross-reactivity and background in secondary antibody detection

Thermo Scientific™ Superclonal™ secondary antibodies represent a breakthrough in recombinant antibody technology. Superclonal™ secondary antibodies are designed to provide precise and accurate detection of mouse, rabbit, and goat primary antibodies in ELISA, western blot, and cell imaging applications.

To produce Superclonal™ secondary antibodies, we employ a proprietary screening and production process that yields specific mixtures of recombinant goat or rabbit secondary antibodies. These antibodies bind with the epitope-specific precision of monoclonal antibodies, while also achieving the multi-epitope coverage (e.g., both heavy and light chains of target IgGs) and sensitivity of polyclonal antibodies. Superclonal™ secondary antibodies are available unconjugated, as well as conjugated with biotin, HRP, and select Alexa Fluor™ dyes; see them all at thermofisher.com/superclonal.

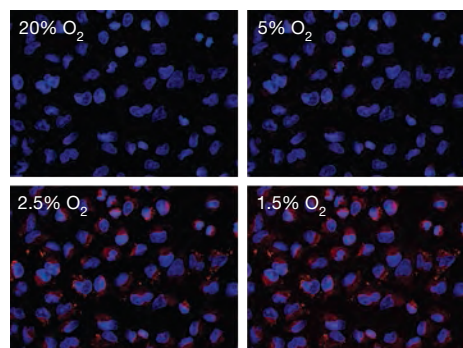


Reduction in nonspecific staining with Superclonal™ secondary antibodies. HeLa cell nucleoli were labeled with anti-nucleostemin primary antibody, which was then detected with the Alexa Fluor™ 488 conjugate (green) of (A) highly cross-adsorbed goat anti-mouse IgG (H+L) antibody, or (B) Superclonal™ goat anti-mouse IgG (H+L) antibody. Superclonal™ secondary antibodies exhibit significantly less cytoplasmic staining, indicating enhanced specificity.

Image-iT™ Hypoxia Reagent: A real-time oxygen sensor for live cells

Image-iT™ Hypoxia Reagent is a fluorogenic, cell-permeant compound for measuring hypoxia in live cells. This reagent is nonfluorescent in an environment with normal oxygen concentrations and becomes increasingly fluorescent as oxygen levels are decreased. Because it responds quickly to a changing environment, Image-iT™ Hypoxia Reagent can serve as a real-time oxygen detector, with a fluorescent signal that increases as atmospheric oxygen levels drop below 5% and decreases if oxygen concentrations increase. These properties make this reagent an ideal tool for detecting hypoxic conditions in tumor cells, 3D cultures, spheroids, neurons, and other live samples. Image-iT™ Hypoxia Reagent is very easy to use; just add it to cell culture medium and image. Find out more at thermofisher.com/hypoxia.

Product	Quantity	Cat. No.
Image-iT™ Hypoxia Reagent	1 mg	H10498

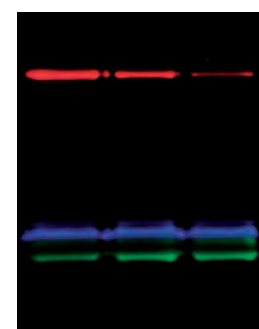


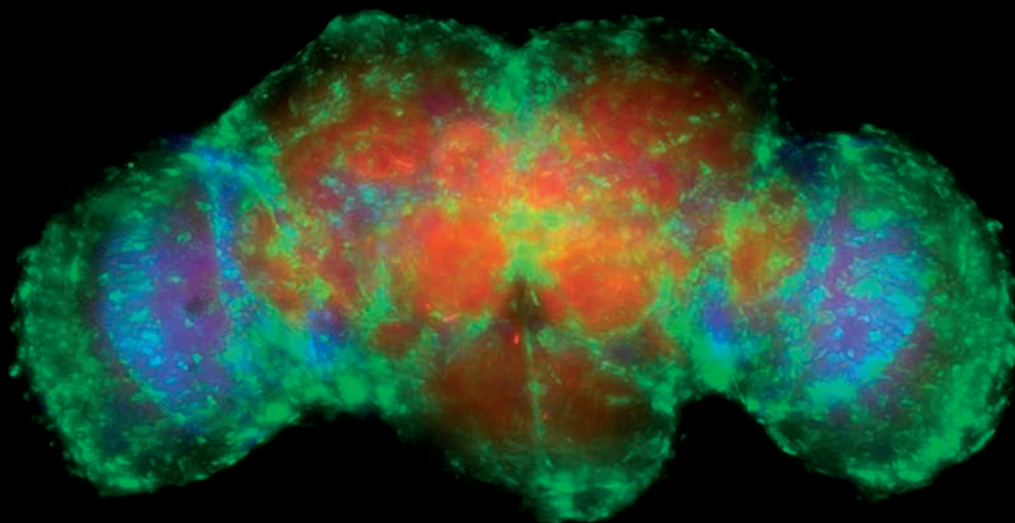
Fluorescence response of cells labeled with the Image-iT™ Hypoxia Reagent as oxygen levels drop. A549 cells were left overnight under normoxic conditions in a CO₂ incubator and then treated with 5 μM Image-iT™ Hypoxia Reagent (red) and NucBlue™ Live Cell Stain (blue) in complete growth medium on an EVOS™ Onstage Incubator at varying O₂ concentrations (20%, 5%, 2.5%, and 1.5%) for 1 hr and imaged on the EVOS™ FL Auto Imaging System.

WesternDot™ primary antibody conjugates for mCherry fusions and His-Tag labels

WesternDot™ primary antibodies are designed to reliably detect mCherry or His-Tag proteins in western blot applications, eliminating the need for secondary antibodies. These intensely fluorescent antibodies enable superior signal-to-noise ratios, as well as detection sensitivities that are comparable with those of ECL-based chemiluminescent methods. Different fluorescent colors of WesternDot™ antibodies can be applied to a single blot and multiple proteins detected simultaneously using standard gel or blot imaging platforms; no stripping and reprobing is required. It's simple to try WesternDot™ antibodies in your current western blot applications; they are compatible with standard membranes, blocking solutions, and buffers. Learn more at thermofisher.com/westerndot.

Simultaneous detection of three different proteins on a single blot using WesternDot™ antibody conjugates. A western blot containing mCherry and GFP lysate from HeLa cells spiked with decreasing quantities of His-tagged protein was probed with WesternDot™ 655 anti-His-Tag (red, Cat. No. W10834), WesternDot™ 800 anti-mCherry (blue, Cat. No. W10831), and chicken anti-GFP (Cat. No. A10262) in conjunction with WesternDot™ 585 goat anti-chicken secondary antibody (green, Cat. No. W10826). The blot was imaged using the Fujifilm™ LAS-4000 gel imager.





A sensitive assay for hyperploidy and cell death in the *Drosophila* brain using the Attune™ Acoustic Focusing Cytometer

Olga Grushko and Laura Buttitta
University of Michigan

Alzheimer's disease (AD), characterized by a progressive loss of cognitive function, is the most prevalent neurodegenerative disorder of aging. A substantial body of literature has documented evidence of cell cycle re-entry and an increase in DNA ploidy in cases of age-induced neurodegeneration and AD [1,2]. Research on human tissue samples has suggested that hyperploidy in neurons may precede clinical diagnosis of AD [3,4]. Thus, cell cycle re-entry and the resulting hyperploidy could be a proximal cause of age-related neurodegeneration, as well as a useful preclinical marker. Dissecting the precise biological significance of cell cycle re-entry in age-related neural decline will be critical to developing new approaches to combat AD.

Figure 1 (above). An aged adult *Drosophila* brain, showing glial-specific GFP expression and actin-selective fluorescent staining. This *Drosophila* brain was dissected from a 50-day-old fly (average lifespan of this strain is 45 days) that expressed nuclear-localized GFP in glial cells (green). The isolated brain was stained with rhodamine phalloidin (red, Cat. No. R415) to label actin and Hoechst™ 33258 (blue, Cat. No. H3569) to label DNA. Image provided by Laura Buttitta and Olga Grushko, University of Michigan.

Developing a model system to study cell cycle re-entry and aging

Extensive literature has reported that cell cycle genes become reactivated in aging brains, and that this reactivation is evolutionarily conserved among diverse species—from flies to humans [5–7]. It has been difficult, however, to observe and quantify cell cycle re-entry of postmitotic cells in the brain due to its rare and potentially transient nature [8,9]. Therefore, its frequency under normal physiological aging conditions has become a matter of debate [3,10–13]. Another barrier to progress in this field has been the difficulty in obtaining aged adult brain samples and monitoring cell cycle re-entry under normal physiological conditions. These challenges, combined with a limited ability to genetically manipulate factors influencing cell cycle re-entry in mammalian models, have hampered investigations.

Progress would be greatly facilitated by the availability of a genetically tractable system that recapitulates the features of age-associated decline in the brain under a rapid lifespan. The simple fruit fly *Drosophila melanogaster* is an attractive model system to study this process because it exhibits age-related neural decline [14], ages on the order of days instead of years, and has well-developed tools for *in vivo* genetic manipulations [15].

Our laboratory is developing genetic tools and fluorescence assays for manipulating cell cycle re-entry in the adult fly brain (Figure 1) and monitoring subsequent effects on DNA ploidy and cell death. Our long-term goal is to understand the contribution of cell cycle misregulation in the brain to age-related neural decline. We want to address several long-standing and important questions in the field, including:

- What causes cell cycle re-entry in the aging brain?
- How do cell cycle re-entry and misregulation affect cell loss and neurodegeneration?
- How does manipulation of cell cycle re-entry impact age-associated neural decline?

Assaying DNA content and cell death with flow cytometry

To begin to investigate these questions, we use a sensitive, high-throughput flow cytometry-based assay to monitor changes in cellular DNA content and cell death in the fly brain (Figure 2). Our method involves dissecting the adult fly brain, dissociating the tissue to a single-cell suspension using gentle trypsinization, and then staining live cells for DNA content with the Vybrant™ DyeCycle™ Violet Stain, a cell-permeant, UV/violet laser-excitable nucleic

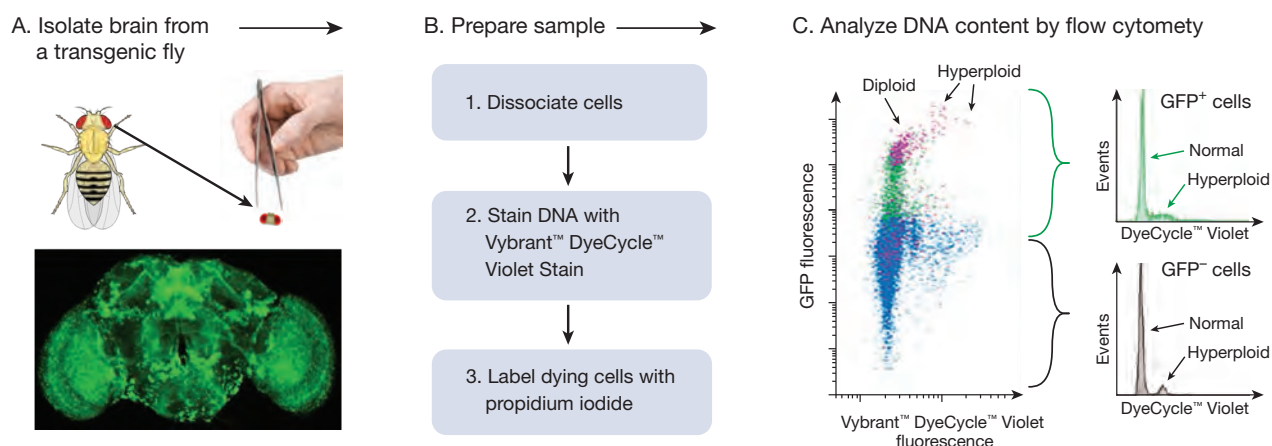


Figure 2. Experimental workflow for examining DNA ploidy and cell death in the aging adult *Drosophila* brain using acoustic focusing cytometry. (A) Individual adult fly brains are dissected; in this case, the strain expresses GFP in the nuclei of adult glial cells. (B) Cells from the isolated brain are dissociated in 100 μ L of a PBS/trypsin solution containing Vybrant™ DyeCycle™ Violet Stain (Cat. No. V35003, 1 μ L/mL) and propidium iodide (PI, Cat. No. P3566, 5 μ L/mL); tissues are quickly triturated by pipetting in a 1.5 mL microcentrifuge tube cap and then transferred to a microcentrifuge tube containing 400 μ L of additional PBS/trypsin/Vybrant™ DyeCycle™ Violet/PI solution and stained for 1 hr. After staining, samples are diluted with 500 μ L of PBS and the microcentrifuge tube is placed in the tube holder and run on the Attune™ Acoustic Focusing Cytometer (with blue/violet lasers) in high-sensitivity mode. Doublets and cell clumps or debris are excluded by comparing DNA height and width [see [16] for details] and removed by gating. (C) A representative dot plot of cells from an aged adult fly brain showing GFP expression (in glial cells) and DNA content (as measured with Vybrant™ DyeCycle™ Violet Stain), with PI-positive dead and dying cells backgated in pink. Here, GFP-positive glial cells show limited hyperploidy but higher levels of cell death, while the non-glial GFP-negative cells (primarily neurons) show less cell death but slightly increased levels of hyperploidy.

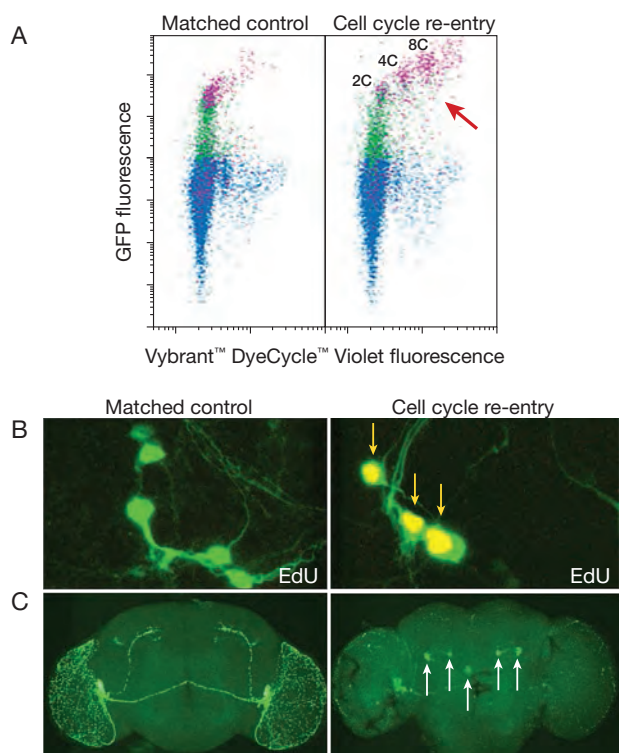


Figure 3. Assessing hyperploidy and cell death in two different cell types of the fly brain. (A) Flies expressing GFP in glial cells were either left untreated (left panel) or induced to re-enter the cell cycle by overexpressing key cell cycle regulators (right panel). Isolated brains were assayed for DNA ploidy and cell death using the workflow described in Figure 2. GFP-expressing glia expressing cell cycle regulators show hyperploidy, including cells exhibiting 4C and 8C DNA content (red arrow). Dead and dying cells incorporate propidium iodide (PI, backgated in pink), and hyperploidy in glia is strongly correlated with PI positivity. (B) Flies expressing GFP in postmitotic neurons were either left untreated (left panels) or induced to re-enter the cell cycle by overexpressing key cell cycle regulators (right panel). After isolating the brains, cell cycle re-entry was confirmed by the incorporation of 5-ethynyl-2'-deoxyuridine (EdU) into newly synthesized DNA with the Click-iT™ EdU Alexa Fluor™ 555 Imaging Kit (yellow arrows, the yellow signal is due to overlap of GFP and Alexa Fluor™ 555 fluorescence; Cat. No. C10338). (C) Pigment-dispersing factor (PDF)-expressing postmitotic neurons (a subset of neurons influencing circadian rhythms in fly brain) were labeled with a mitochondrial-localized GFP and left untreated (left panel) or induced to re-enter the cell cycle by overexpressing key cell cycle regulators (right panel). Neurons that re-enter the cell cycle exhibit hallmarks associated with neurodegeneration, including loss of mitochondria and aberrant mitochondrial clumping (white arrows).

acid dye [16]. We also measure cell death, the eventual consequence of aging-related neural decline, using the live cell-impermeant nucleic acid dye propidium iodide (PI). The Attune™ Acoustic Focusing Cytometer allows us to measure rare events and identify small populations of cells in the fly brain, on the scale of a single brain.

Figure 2C shows data from an experiment in which adult fly brains expressing GFP in glial cells were dissected, dissociated

into single cells, stained with Vybrant™ DyeCycle™ Violet Stain, and analyzed on the Attune™ Acoustic Focusing Cytometer (with blue/violet lasers) in high-sensitivity mode. After excluding doublets, cell clumps, and debris by gating (described in [16]), we used a dot plot of GFP fluorescence vs. DNA content to identify diploid and hyperploid cells, with PI-positive dead or dying cells backgated in pink.

In a normal aged adult fly brain, GFP-labeled glial cells exhibit limited hyperploidy but increased levels of cell death, while GFP-negative neural cells show a slight increase in hyperploidy, but less cell death. The relative levels of hyperploidy for the GFP-labeled glia and GFP-negative neurons can also be shown as a traditional DNA content histogram. Importantly, our use of individual, isolated fly brains allows us to capture any variations in DNA ploidy and cell death between isogenic animals, in order to estimate frequencies of potentially rare increases in ploidy in specific populations carrying mutations associated with neurodegeneration.

Genetically manipulating cell cycle regulators

We use the binary Gal4/UAS system to activate gene expression in specific cell types in the *Drosophila* brain [17]. To force cell cycle re-entry, we express a combination of cell cycle regulators—cyclin G1, cyclin D, its partner kinase Cdk4, and the cell cycle transcriptional activator E2F—which we have previously reported can reverse cell cycle exit in postmitotic tissues when overexpressed [18]. Thus, we can simultaneously activate cell cycle genes with the Gal4/UAS system, induce GFP or another fluorescent marker in a cell type-specific manner, and monitor the ploidy and death of subpopulations of cells in the adult fly brain.

Figure 3A shows a pair of GFP fluorescence vs. DNA content dot plots comparing control cells expressing GFP under a glial-specific promoter, to GFP-positive glial cells that have been forced to re-enter the cell cycle. The cell population forced to re-enter the cell cycle exhibits increased DNA hyperploidy, including 4C and 8C cells, which is also strongly correlated with PI positivity.

We can also force cell cycle re-entry in postmitotic neurons, such as those shown in Figure 3B, and observe hallmarks of active cell cycling via incorporation of 5-ethynyl-2'-deoxyuridine (EdU) and subsequent detection using the Click-iT™ EdU Alexa Fluor™ 555 Imaging Kit. Forced cell cycle re-entry in postmitotic neurons leads to phenotypes consistent with neurodegeneration, such as mitochondrial clumping and loss [19] (Figure 3C).

Watch the JoVE video on cell cycle analysis of *Drosophila* tissues



Follow along with the protocol for “Live cell cycle analysis of *Drosophila* tissues using the Attune Acoustic Focusing Cytometer and Vybrant DyeCycle Violet DNA Stain” by Kerry Flegel, Dan Sun, Olga Grushko, Yiqin Ma, and Laura Buttitta (Molecular, Cellular, and Developmental Biology, University of Michigan) at [jove.com/video/50239/live-cell-cycle-analysis-drosophila-tissues-using-attune-acoustic](https://www.jove.com/video/50239/live-cell-cycle-analysis-drosophila-tissues-using-attune-acoustic) (a subscription to JoVE is required). In this 11-minute video, the authors discuss fly dissection, tissue dissociation, DNA staining, and subsequent analysis by acoustic focusing cytometry. Their cell cycle analysis protocol provides a method for determining relative cell size, cell number, and DNA content, as well as cell type via lineage tracing or cell type-specific fluorescent protein expression. This video has been viewed thousands of times by universities and research labs worldwide.

Future directions

While hyperploidy has been observed in aged human brains and in cases of AD, it remains unclear whether hyperploidy is restricted to neurons or glia, and which cell types are responsible for the neural decline. Glia play a critical support role for maintaining neuronal survival in the brain, and disruption of their quiescence may have huge impacts on the brain. Indeed, cell cycle re-entry in glia may lead to neurodegenerative phenotypes in *Drosophila* [20,21].

Using the adult fly brain as our model system, we can both assay and manipulate cell cycle re-entry in multiple cell types under physiological aging conditions. Our future investigations aim to establish a new model system for examining the role of cell cycle re-entry in age-related neural decline. If successful, our work will provide information about how aging impacts critical cell cycle controls in the brain, which may suggest novel approaches to combat age-related declines in cognitive function. ■

Laura Buttitta, PhD, is an assistant professor in the Department of Molecular, Cellular, and Developmental Biology at the University of Michigan. Her lab studies how the cell cycle is shut off in quiescent cells, such as differentiated or stem cells, using both *Drosophila* and mammalian cell systems. Olga Grushko, PhD, a research specialist at the University of Michigan, is studying the adult *Drosophila* brain, neuronal populations involved in feeding behaviors, and neurodegeneration. Correspondence can be sent to buttitta@umich.edu.

References

- Herrup K, Yang Y (2007) Cell cycle regulation in the postmitotic neuron: oxymoron or new biology? *Nat Rev Neurosci* 8:368–378.
- Khurana V, Feany MB (2007) Connecting cell-cycle activation to neurodegeneration in *Drosophila*. *Biochim Biophys Acta* 1772:446–456.
- Arendt T, Bruckner MK, Mosch B et al. (2010) Selective cell death of hyperploid neurons in Alzheimer's disease. *Am J Pathol* 177:15–20.
- Yang Y, Geldmacher DS, Herrup K (2001) DNA replication precedes neuronal cell death in Alzheimer's disease. *J Neurosci* 21:2661–2668.
- McCarroll SA, Murphy CT, Zou S et al. (2004) Comparing genomic expression patterns across species identifies shared transcriptional profile in aging. *Nat Genet* 36:197–204.
- Lu T, Pan Y, Kao SY et al. (2004) Gene regulation and DNA damage in the ageing human brain. *Nature* 429:883–891.
- Yang Y, Mufson EJ, Herrup K (2003) Neuronal cell death is preceded by cell cycle events at all stages of Alzheimer's disease. *J Neurosci* 23:2557–2563.
- Mosch B, Morawski M, Mittag A et al. (2007) Aneuploidy and DNA replication in the normal human brain and Alzheimer's disease. *J Neurosci* 27:6859–6867.
- von Trotha JW, Egger B, Brand AH (2009) Cell proliferation in the *Drosophila* adult brain revealed by clonal analysis and bromodeoxyuridine labelling. *Neural Dev* 4:9.
- Bauer S, Patterson PH (2005) The cell cycle–apoptosis connection revisited in the adult brain. *J Cell Biol* 171:641–650.
- Fischer HG, Morawski M, Bruckner MK et al. (2012) Changes in neuronal DNA content variation in the human brain during aging. *Aging Cell* 11:628–633.
- Swartz FJ, Bhatnagar KP (1981) Are CNS neurons polyploid? A critical analysis based upon cytophotometric study of the DNA content of cerebellar and olfactory bulb neurons of the bat. *Brain Res* 208:267–281.
- Pack SD, Weil RJ, Vortmeyer AO et al. (2005) Individual adult human neurons display aneuploidy: detection by fluorescence *in situ* hybridization and single neuron PCR. *Cell Cycle* 4:1758–1760.
- Martinez VG, Javadi CS, Ngo E et al. (2007) Age-related changes in climbing behavior and neural circuit physiology in *Drosophila*. *Dev Neurobiol* 67:778–791.
- Duffy JB (2002) GAL4 system in *Drosophila*: a fly geneticist's Swiss army knife. *Genesis* 34:1–15.
- Flegel K, Sun D, Grushko O et al. (2013) Live cell cycle analysis of *Drosophila* tissues using the Attune Acoustic Focusing Cytometer and Vybrant DyeCycle Violet DNA Stain. *J Vis Exp* 75:e50239.
- Brand AH, Perrimon N (1993) Targeted gene expression as a means of altering cell fates and generating dominant phenotypes. *Development* 118:401–415.
- Buttitta LA, Katzaroff AJ, Perez CL et al. (2007) A double-assurance mechanism controls cell cycle exit upon terminal differentiation in *Drosophila*. *Dev Cell* 12:631–643.
- Wang X, Su B, Lee HG et al. (2009) Impaired balance of mitochondrial fission and fusion in Alzheimer's disease. *J Neurosci* 29:9090–9103.
- Petersen AJ, Rimkus SA, Wassarman DA (2012) ATM kinase inhibition in glial cells activates the innate immune response and causes neurodegeneration in *Drosophila*. *Proc Natl Acad Sci U S A* 109:E656–664.
- Rimkus SA, Katzenberger RJ, Trinh AT (2008) Mutations in *String/CDC25* inhibit cell cycle re-entry and neurodegeneration in a *Drosophila* model of Ataxia telangiectasia. *Genes Dev* 22:1205–1220.

Product	Quantity	Cat. No.
Attune™ NxT Acoustic Focusing Cytometer, Blue/Violet	1 system	A24862
Click-iT™ EdU Alexa Fluor™ 555 Imaging Kit	1 kit	C10338
Propidium Iodide, 1 mg/mL solution in water	10 mL	P3566
Vybrant™ DyeCycle™ Violet Stain	200 µL	V35003

Isolation and characterization of exosomes using magnetic beads

Ketil W. Pedersen¹, Bente Kierulf¹, Morten P. Oksvold^{2,3}, Mu Li¹,
Alexander V. Vlassov¹, Norbert Roos⁴, Anette Kullmann¹, Axl Neurauter¹

Exosomes are extracellular vesicular structures (50–150 nm in diameter) secreted by all cells in culture and found in all body fluids investigated to date [1]. Exosomes function in diverse biological processes, including apoptosis, antigen presentation, angiogenesis, inflammation, and coagulation [2,3]. They have been observed to activate signaling pathways, as well as to deliver nucleic acids to distant cells [4–6]. Furthermore, tumor-derived exosomes can enhance cancer progression by transferring oncogenes from tumor cells to cells lacking the oncogene [7].

Both the concentration and composition of exosomes can vary significantly during disease. The isolation and characterization of exosomes from body fluids and cell culture systems will provide important information that may be useful for early disease detection, monitoring of disease status, and the development of effective treatments for cancer, inflammation, and autoimmune diseases. Further insight into exosome biology may also accelerate the use of these nanovesicles in regenerative medicine and vaccination research and increase the efficacy of therapeutic antibodies.

Improved exosome isolation protocols under development

The established exosome isolation protocol is differential centrifugation with a final ultracentrifugation step, although density gradient or cushion [8], size exclusion [9], or precipitation [10–12] methods are also employed. Differential ultracentrifugation, however, is time consuming, requires expensive equipment, and cannot discriminate between exosome subpopulations or other particles with similar size and density such as protein aggregates, lipids, and miscellaneous nucleic acid complexes. To obtain ultrapure exosomes or to isolate potential exosome subpopulations, an immunomagnetic isolation strategy can be applied by targeting exosomal surface markers [13,14].

The aim of this study was to establish a direct method for fast, efficient, and selective isolation of exosomes from cell culture supernatants that is compatible with a wide range of downstream applications. Here we describe the use of magnetic beads coated with antibodies against the tetraspanins CD9 or CD81—common exosomal markers—to isolate and characterize pre-enriched exosomes derived from SW480 (human colon adenocarcinoma) and Jurkat (human T lymphocyte) cells. Critical factors such as volume, time, and exosome concentrations were addressed in order to establish optimal and comparable isolation conditions. In addition, we have developed a method for isolating exosomes *directly* from cell culture medium using magnetic beads. Direct isolation methods have the potential not only to shorten the workflow, but also to reduce any artifacts or contamination that can result from enrichment procedures, producing exosomes that can be further characterized with sensitive techniques such as mass spectrometry.

Analysis of exosome markers in pre-enriched exosome samples

Typically, exosome samples are prepared using either differential ultracentrifugation or precipitation. Figure 1 shows the analysis of SW480 cell culture medium that was harvested after 24 hours, followed by centrifugation to remove debris and precipitation using the Total Exosome Isolation Reagent. As expected, the exosomes contained full-length mRNA (GAPDH and ACTB), rRNA (18S), and miRNA (Let7a and miR16), which are typical exosome cargo [15] (Figure 1A). In addition, the exosomes exhibited a size distribution comparable with that of standard samples prepared by ultracentrifugation [16] (Figure 1B), and they had the common exosome surface marker CD81 [17,18], as confirmed by anti-human CD81 antibodies and electron microscopy (Figure 1C). The exosome markers CD9 and CD81 were also detected by western blotting (Figure 1D).

Pre-enriched vesicles were then identified by flow cytometry using magnetic beads as a solid support detectable by the instrument. For equal binding kinetics, the ratio of number of magnetic beads to isolation volume was kept constant. Pre-enriched CD9-positive adenocarcinoma-derived exosomes were isolated using magnetic beads coated with anti-human CD9 antibodies followed

¹Thermo Fisher Scientific in Oslo, Norway and Austin, Texas, United States;

²Department of Immunology, Institute for Cancer Research, Oslo University Hospital, Norway; ³Centre for Cancer Biomedicine, University of Oslo, Norway; ⁴Department of Biosciences, Section for Physiology and Cell Biology, University of Oslo, Norway.

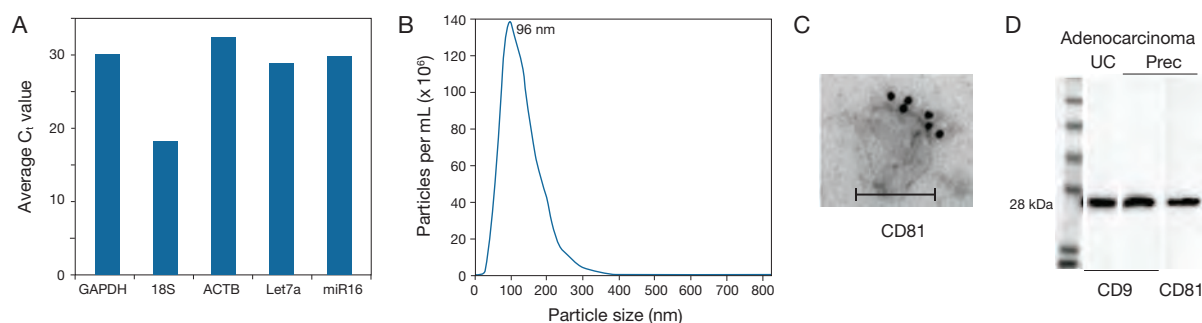


Figure 1. Analysis of precipitated exosomes obtained with the Total Exosome Isolation Reagent. (A) Precipitated exosomes released from adenocarcinoma [SW480] cells and isolated with the Total Exosome Isolation Reagent (Cat. No. 4478359) were analyzed for RNA characteristic of exosomes—mRNA (GAPDH, ACTB), rRNA (18S), and miRNA (Let7a, miR16)—by qRT-PCR. Average C_t values for three independent experiments are shown ($n = 3$). (B) Precipitated exosomes from SW480 culture medium were analyzed by nanotrack analysis (size distribution) on the NanoSight™ LM10 instrument. The size distribution and concentration of total exosomes resuspended in PBS are shown. (C) Immunolabeling of exosomes derived from SW480 cells. Bar = 100 nm. (D) Western blot analysis of ultracentrifuged (UC) and precipitated (Prec) exosomes detected with antibodies against exosomal surface proteins CD9 (Cat. No. 10626D) and CD81 (Cat No. 10630D).

by CD9 staining. The side/forward scatter plot demonstrates the presence of magnetic beads (Figure 2A, red data points). Isolated exosomes stained with isotypic antibody show the background autofluorescence of the beads (Figure 2B, gray peak) compared with the specific fluorescent signal exhibited by the bead-isolated exosomes stained with the R-phycoerythrin (PE) conjugate of anti-human CD9 antibody (Figure 2B, red peak). Isolation efficiency was confirmed by flow cytometric analysis of the remaining exosomes in the supernatant post-isolation. Increasing amounts of magnetic beads were used for isolation, starting with amounts equivalent to what is used for flow cytometry (1x) up to the amount of beads recommended for western blotting (25x) (Figure 2C). The flow cytometry results were confirmed by western blot analysis of exosomes prior to isolation and after isolating with anti-CD9 antibody-coated magnetic beads (Figure 2D).

Direct isolation of exosomes from cell culture medium

Directly isolating exosomes from cell culture medium without any pre-enrichment steps would provide a fast and scalable protocol and offer several advantages for downstream applications. We investigated the use of the immunomagnetic separation method with cell culture supernatants that had not been pre-enriched for exosomes. Specifically, we used anti-human CD81 antibody-coated magnetic beads for the isolation of exosomes from T lymphocyte (Jurkat) cell culture (after an initial low-speed centrifugation step to remove cells and cell debris). Several factors were investigated. First, the impact of the volume of exosome-containing cell culture medium during isolation was addressed. Increasing the amount of exosome-containing cell culture medium (200 μ L, 400 μ L, 800 μ L) while keeping the amount of magnetic beads constant (20 μ L) provided a nonlinear (+) dose-response curve (Figure 3A). At very

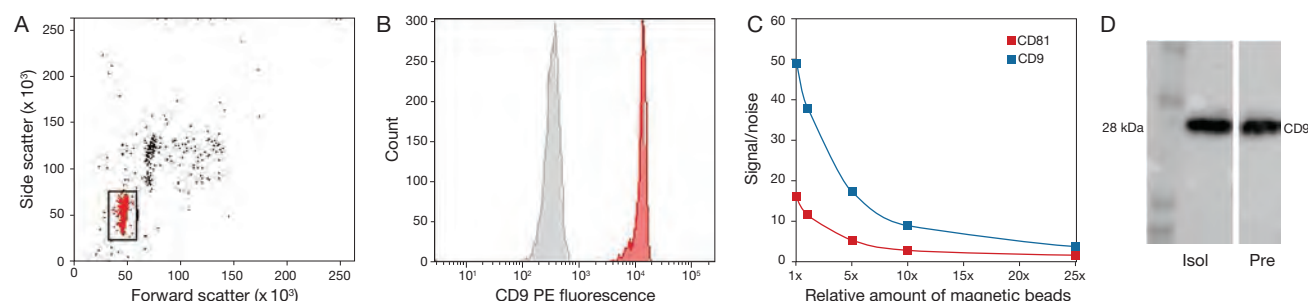


Figure 2. Flow cytometric analysis of exosomes isolated with magnetic beads targeting CD9. (A) Scatter plot of exosomes isolated with magnetic beads coated with anti-human CD9 antibody (Cat. No. 10620D); gating is shown. (B) CD9⁺ exosomes isolated with magnetic beads were stained with fluorescent anti-human CD9 antibody (CD9-PE, red peak) or an isotype control (gray peak). (C) Depletion efficiency was measured by flow cytometry (signal/noise) of the supernatant after isolation for western blotting. 25x represents the amount of magnetic beads used for western blotting. (D) Exosomes were subjected to western blot analysis with anti-CD9 antibody (Cat. No. 10626D) prior to (Pre) and post (Isol) isolation with magnetic beads.

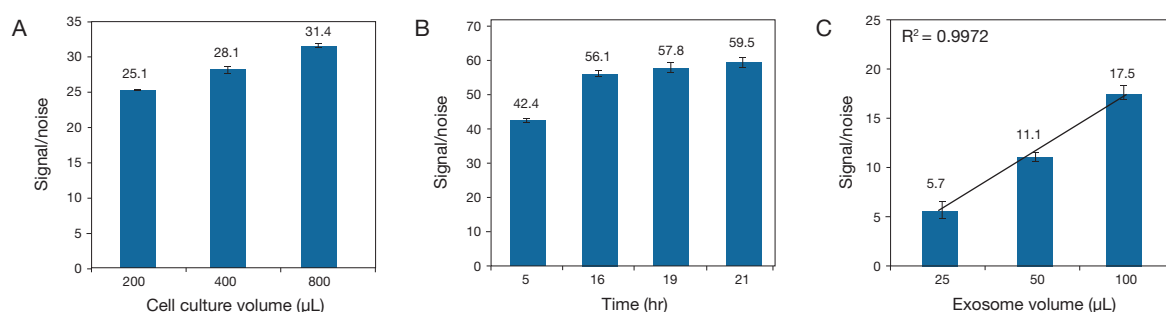


Figure 3. Flow cytometric analysis of the effects of incubation volume, incubation time, and exosome input on exosome isolation. Exosomes derived from Jurkat cells were isolated using magnetic beads coated with anti-human CD81 antibody (Cat. No. 10622D), followed by fluorescent anti-human CD81 antibody (CD81-PE) staining. Samples were then analyzed by flow cytometry and presented as signal/noise. **(A)** CD81⁺ exosomes were isolated from 200 µL, 400 µL, or 800 µL of cell culture medium using 20 µL of magnetic beads. **(B)** CD81⁺ exosomes were isolated from 100 µL of cell culture medium after incubation with 20 µL of magnetic beads for 5, 16, 19, or 21 hr at 4°C. **(C)** CD81⁺ exosomes were isolated from 25 µL, 50 µL, or 100 µL of added exosomes in a 100 µL total volume using 20 µL of magnetic beads.

high volumes, the reduced concentration of magnetic beads resulted in lower binding kinetics. Second, we looked at incubation time. Increasing incubation time with a fixed amount of exosome-containing cell culture medium and magnetic beads produced a nonlinear (+) dose-response curve (Figure 3B). Lastly, we found that increasing the amount of exosomes while keeping the volume of cell culture medium and the amount of magnetic beads constant resulted in a linear (+) dose-response curve (Figure 3C).

The optimized experimental conditions were then used for the direct isolation of exosomes from cell culture medium, which were then analyzed by flow cytometry. Adenocarcinoma (SW480)-derived exosomes were isolated directly using anti-CD9 antibody-coated magnetic beads and compared with exosome samples prepared either by differential ultracentrifugation or by precipitation. To enable direct comparison of the flow analysis, the exosome input was normalized for the three ways of processing conditioned cell

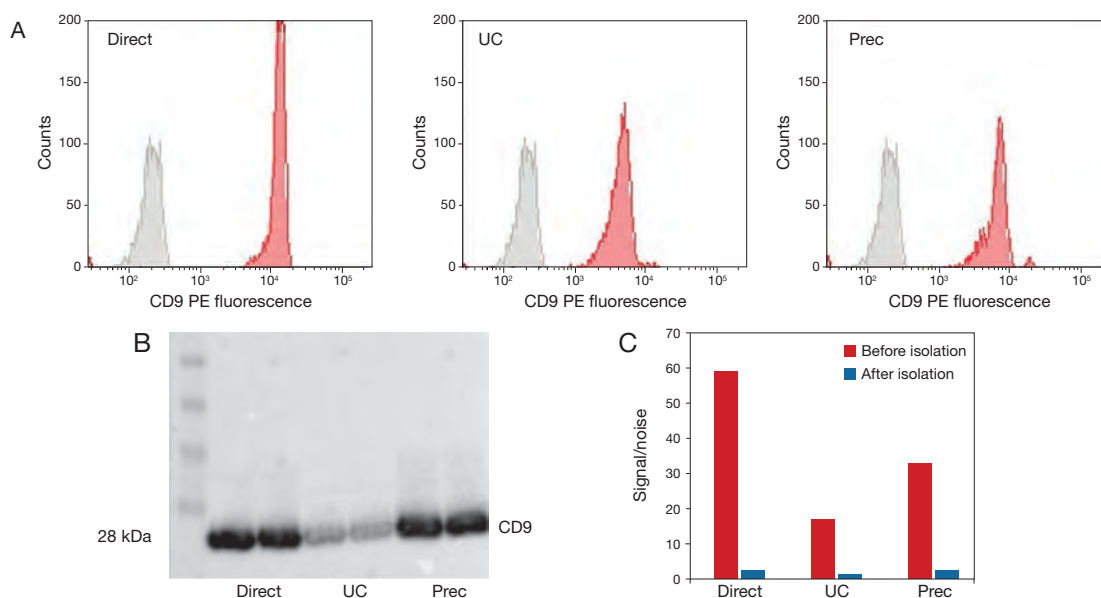


Figure 4. Flow cytometric analysis of CD9-positive adenocarcinoma (SW480)-derived exosomes isolated with magnetic beads directly from cell culture medium (Direct) or after pre-enrichment by ultracentrifugation (UC) or precipitation (Prec). **(A)** The three different exosome preparations were analyzed by flow cytometry after staining with fluorescent anti-human CD9 antibodies (CD9-PE, red peak) or an isotype control (gray peak). **(B)** Western blot confirmation of the results obtained by flow cytometry. **(C)** Exosomes were isolated for western blotting using anti-CD9 antibody-coated magnetic beads (25x the amount of beads used for flow cytometric analysis, Cat. No. 10620D), and the remaining supernatant was subjected to a second round of exosome capture for flow cytometric analysis as described above. The red and blue bars represent the flow analysis pre- and post-exosome isolation for western blotting, respectively.

culture medium based on the concentration factor achieved for ultracentrifugation and precipitation, respectively. All three exosome preparation methods were then analyzed by flow cytometry (Figure 4A) and western blotting (Figure 4B) using fluorescent antibodies against CD9. Densitometry analysis showed that the exosome yields for the pre-enriched (by differential ultracentrifugation or precipitation) preparations were somewhat lower than those of the directly isolated preparations, indicating loss of exosomes during pre-enrichment steps. The isolation efficiencies of the three methods were confirmed by subjecting the supernatants remaining after initial exosome isolation to a second round of isolation (Figure 4C).

Advantages of immunomagnetic isolation protocols

The isolation and analysis of nanometer-sized exosomes is challenging. Today the general approach for exosome isolation is differential ultracentrifugation—though the protocol is not rigorously standardized—requiring several labor-intensive steps and costly equipment. Moreover, differential ultracentrifugation methods increase the risk for exosome loss and fail to discriminate well between exosomes and contaminating structures such as larger vesicles and protein/lipid aggregates [19].

By including magnetic beads coated with antibodies specific for exosome surface proteins in the isolation protocol after

pre-enrichment, we can further enhance the purity of the exosome preparation. We also demonstrate an alternative, optimized workflow for direct exosome isolation with magnetic beads that omits the pre-enrichment step altogether. Direct immunomagnetic isolation requires minimal hands-on time and produces highly purified exosome preparations with minimal loss, enabling downstream analysis and future automation opportunities. ■

Morten P. Øksvold and Norbert Roos of the University of Oslo are collaborating on the isolation and characterization of exosomes with Ketil W. Pedersen, Bente Kierulf, Mu Li, Alexander V. Vlassov, Anette Kullmann, and Axl Neurauter from Thermo Fisher Scientific (Oslo, Norway and Austin, Texas, United States). Dr. Øksvold's research is focused on the biology of B cell lymphoma; Dr. Roos studies viral particles, including viral assembly and membrane trafficking. Correspondence can be sent to axl.neurauter@thermofisher.com.

Product	Quantity	Cat. No.
DynaMag™-2 Magnet	1 each	12321D
Exosome CD9 Monoclonal Antibody, for western blots	200 µL	10626D
Exosome CD81 Monoclonal Antibody, for western blots	200 µL	10630D
Exosome-Human CD9 Flow Detection Reagent (from cell culture)	2 mL	10620D
Exosome-Human CD81 Flow Detection Reagent (from cell culture)	2 mL	10622D
Total Exosome Isolation Reagent (from cell culture medium)	50 mL	4478359

References

- Bobrie A, Colombo M, Raposo G et al. (2011) Exosome secretion: molecular mechanisms and roles in immune responses. *Traffic* 12:1659–1668.
- Thery C, Zitvogel L, Amigorena S (2002) Exosomes: composition, biogenesis and function. *Nat Rev Immunol* 2:569–579.
- Janowska-Wieczorek A, Wysoczynski M, Kijowski J et al. (2005) Microvesicles derived from activated platelets induce metastasis and angiogenesis in lung cancer. *Int J Cancer* 113:752–760.
- Belting M, Wittrup A (2008) Nanotubes, exosomes, and nucleic acid-binding peptides provide novel mechanisms of intercellular communication in eukaryotic cells: implications in health and disease. *J Cell Bio* 183:1187–1191.
- Pegtel DM, van de Garde MD, Middeldorp JM (2011) Viral miRNAs exploiting the endosomal-exosomal pathway for intercellular cross-talk and immune evasion. *Biochim Biophys Acta* 1809:715–721.
- Valadi H, Ekstrom K, Bossios A et al. (2007) Exosome-mediated transfer of mRNAs and microRNAs is a novel mechanism of genetic exchange between cells. *Nat Cell Biol* 9:654–659.
- Al-Nedawi K, Meehan B, Micallef J et al. (2008) Intercellular transfer of the oncogenic receptor EGFRvIII by microvesicles derived from tumour cells. *Nat Cell Biol* 10:619–624.
- Thery C, Amigorena S, Raposo G et al. (2006) Isolation and characterization of exosomes from cell culture supernatants and biological fluids. *Curr Protoc Cell Biol* Chapter 3:Unit 3.22.
- Cheruvanky A, Zhou H, Pisitkun T et al. (2007) Rapid isolation of urinary exosomal biomarkers using a nanomembrane ultrafiltration concentrator. *Am J Physiol Renal Physiol* 292:F1657–1661.
- Li Q, Eades G, Yao Y et al. (2014) Characterization of a stem-like subpopulation in basal-like ductal carcinoma in situ (DCIS) lesions. *J Biol Chem* 289:1303–1312.
- Munoz JL, Bliss SA, Greco SJ et al. (2013) Delivery of functional anti-miR-9 by mesenchymal stem cell-derived exosomes to glioblastoma multiforme cells conferred chemosensitivity. *Mol Ther Nucleic Acids* 2:e126.
- Zeng L, Wang G, Umharino D et al. (2013) Histone deacetylase 3 unconventional splicing mediates endothelial-to-mesenchymal transition through transforming growth factor beta2. *J Biol Chem* 288:31853–31866.
- Chugh PE, Sin SH, Ozgur S et al. (2013) Systemically circulating viral and tumor-derived microRNAs in KSHV-associated malignancies. *PLoS Pathog* 9:e1003484.
- Clayton A, Court J, Navabi H et al. (2001) Analysis of antigen presenting cell derived exosomes, based on immuno-magnetic isolation and flow cytometry. *J Immunol Methods* 247:163–174.
- Zeringer E, Li M, Barta T et al. (2013) Methods for the extraction and RNA profiling of exosomes. *World J Methodol* 3:11–18.
- Øksvold MP, Kullmann A, Forfang L et al. (2014) Expression of B-cell surface antigens in subpopulations of exosomes released from B-cell lymphoma cells. *Clin Ther* 36:847–862.e1.
- Ericsson M, Cudmore S, Shuman S et al. (1995) Characterization of ts 16, a temperature-sensitive mutant of vaccinia virus. *J Virol* 69:7072–7086.
- Yoshioka Y, Konishi Y, Kosaka N et al. (2013) Comparative marker analysis of extracellular vesicles in different human cancer types. *J Extracell Vesicles* 2.
- Tauro BJ, Greening DW, Mathias RA et al. (2012) Comparison of ultracentrifugation, density gradient separation, and immunoaffinity capture methods for isolating human colon cancer cell line LIM1863-derived exosomes. *Methods* 56:293–304.

Few and far between

Tools and strategies for rare-event detection using flow cytometry.

The ability to accurately detect and analyze rare cells in a cell population is critical, not only for the study of disease progression but also for our understanding of key pathways in normal development. Flow cytometry is the method of choice for detecting rare-cell populations—including stem cells, circulating endothelial cells, circulating tumor cells, and residual disease cells—in blood, bone marrow, and a wide variety of other samples. Thanks to technological advances in instrumentation combined with better detection reagents and more sophisticated analysis strategies, the identification of rare cells at frequencies as low as 0.0001% has been reported.

Flow cytometry offers several advantages for the identification, enumeration, and characterization of rare cells. Foremost among these is the ability to perform multiple quantitative measurements on each cell in a cell population, and to subsequently sort these cells for further downstream testing. The availability of flow cytometers with multiple lasers and detection channels, in conjunction with the development of new fluorophores and conjugates that span the visible to near-infrared spectrum, has allowed for improved panel design in multiplex assay protocols (see “Flow cytometry panel design: The basics” on page 20). These multiparameter measurements increase assay specificity while also providing a strategy for identifying and eliminating cells from further analysis (e.g., see “Gating strategies

for maximizing assay specificity” on the next page), each of which is critical to the detection of rare cells.

Flow cytometry, however, also poses several technical limitations for rare-cell detection, including the time required to process large sample volumes (or, alternatively, to perform enrichment techniques prior to analysis), and the lack of visual confirmation of cell identity. Several excellent review articles discuss these challenges in detail [1,2]. Here we focus on a few major obstacles in rare-cell detection, specific strategies to address them, and examples of successful rare-cell analysis by flow cytometry both from recently published reports and from our own labs. We also demonstrate that acoustic focusing cytometry can dramatically increase sample acquisition rates compared with conventional flow cytometry, enabling a larger number of rare cells to be analyzed in a single experiment.

How many events must be acquired?

In flow cytometry, an “event” is defined as a single particle detected by the instrument. The term “rare” generally refers to a frequency of 0.01% and below. Accurate detection of rare-cell events using flow cytometry requires the ability to detect single cells with specific characteristics in a heterogeneous population of cells. This detection can be additionally complicated by the challenge of detecting the cells of interest in a limited sample or in the presence of cell debris or other artifacts of sample preparation. Minimal sample preparation is recommended, to avoid these artifacts and minimize cell loss. “No-lyse/no-wash” or “lyse/no-wash” procedures can help maintain the cells’ native characteristics while maximizing recovery of the rare population (see “First, do no harm” on page 28). For example, the Invitrogen™ High-Yield Lyse Solution is a premixed, fixative-free erythrocyte-lysing solution for flow cytometry that eliminates red cells from whole blood without a subsequent wash step, minimizing loss of rare blood cell populations [3].

When investigating a rare population of cells, it may be necessary to acquire millions of events to obtain a sufficient number of cells for statistically significant detection. The number of events needed for analysis depends on three main factors: the ratio of cells to debris in the sample; the signal-to-noise ratio of the detected cells compared to background fluorescence; and the frequency of

Watch the Science/AAAS webinar on rare-cell detection and analysis



For more information on how to maximize your rare-event studies, view the webinar “Overcoming challenges in cellular analysis: Multiparameter analysis of rare cells” by Andrea Cossarizza (University of Modena and Reggio Emilia School of Medicine, Italy) and David Cousins (University of Leicester, United Kingdom) at webinar.sciencemag.org/webinar/archive/overcoming-challenges-cellular-analysis. In this webinar, the speakers discuss advances in flow cytometry that have improved the detection of rare-cell events and provide examples of the isolation and analysis of innate lymphoid cells (ILCs), circulating antigen-specific lymphocytes, and innate-like cells such as natural killer T cells and circulating endothelial cells (CECs).

Table 1. Number of cells required to achieve a given precision in rare-event analysis. Adapted from Allan AL, Keeney M (2010) *J Oncol* 426218.

Desired CV [%]	1	5	10	20	40	
Number of events of interest* (r)	10,000	400	100	25	6	
When occurring at a frequency of [%]	1 : n	Total number of events that must be collected †				
10	10	10 ⁵	4 × 10 ³	10 ³	2.5 × 10 ²	6.25 × 10 ¹
1	100	10 ⁶	4 × 10 ⁴	10 ⁴	2.5 × 10 ³	6.25 × 10 ²
0.1	1,000	10 ⁷	4 × 10 ⁵	10 ⁵	2.5 × 10 ⁴	6.25 × 10 ³
0.01	10,000	10 ⁸	4 × 10 ⁶	10 ⁶	2.5 × 10 ⁵	6.25 × 10 ⁴
0.001	100,000	10 ⁹	4 × 10 ⁷	10 ⁷	2.5 × 10 ⁶	6.25 × 10 ⁵
0.00001 ‡	10,000,000	10 ¹¹	4 × 10 ⁹	10 ⁹	2.5 × 10 ⁸	6.25 × 10 ⁷

*For cell-based assays such as flow cytometry, a simple calculation can be used to determine the size of the database or sample that will provide a given precision: $r = (100/CV)^2$, where r is the number of events meeting the required criterion, and CV is the coefficient of variation of a known positive control. † With a WBC count in the low-normal range (5×10^9 cells/L), 10 mL of blood would contain 5×10^7 events. ‡ Estimated frequency of CTCs in the peripheral blood of cancer patients.

the cell population of interest in the sample. Poisson statistics apply when counting randomly distributed populations, where precision increases as more events are acquired [1]. To determine the size of the sample (number of cells) that will provide a given precision, the equation $r = (100/CV)^2$ is used, where r is the number of cells meeting the defined criterion of the rare event, and CV is the coefficient of variation of a known positive control. Table 1 shows the number of events required to achieve various levels of precision in rare-cell analysis [4].

Strategies for optimizing instrument sensitivity

For extremely rare cell populations such as circulating endothelial cells—occurring at a frequency of 0.01–0.0001% in a background of peripheral mononuclear cells—1 million to 10 million cells must be analyzed. Acquiring this many cells can pose challenges, both in terms of the volume of sample (e.g., blood) and the instrument time required, as well as the size of the data files for analysis. As discussed below, acoustic focusing cytometry can mitigate some of these issues because its detection speeds (up to 35,000 events

per second) and sample flow rates (up to 1,000 μ L per minute) are dramatically higher than those of conventional hydrodynamic focusing cytometers, allowing more cells and a larger sample volume to be analyzed without compromising data (Table 2).

Two other often-overlooked factors to consider when optimizing the sensitivity of a flow cytometry assay are the cleanliness of the instrument and the integrity of the sample. It is important to make sure the instrument and fluids used are clean and free of particles that could contribute falsely to the rare population. Additionally, during acquisition, it can be helpful to include time as a parameter, looking for any bursts or breaks of data during acquisition that may indicate a problem with the sample (such as clumping) or with the fluidics of the instrument.

Gating strategies for maximizing assay specificity

High assay specificity is a critical requirement for detecting a maximum number of true positive cells while at the same time minimizing false-positive and false-negative events. Phenotypic differences between the rare cells and the background cells can be exploited by using markers that are specific to each population. Increasing the number of markers that distinguish rare cells can lead to enhanced assay sensitivity and specificity; this multiparameter gating strategy is facilitated by a flow cytometer with multiple lasers and 10 or more fluorescence detectors, such as the Attune™ NxT Acoustic Focusing Cytometer (see page 19).

To maximize detection of the rare event, more than one fluorescence parameter should be used to positively identify the cell of interest (compound gating). Likewise, there should be at least one fluorescence parameter for which the rare event is negative (negative gating). This negative channel, which is used to exclude a →

Table 2. Comparison of collection rates obtained using hydrodynamic focusing cytometry and acoustic focusing cytometry.

Instrument collection rate	Time to acquire 10 ⁶ granulocyte events*	Relative rate
Hydrodynamic focusing at "High" flow rate	63 min 33 sec	—
Acoustic focusing at 200 μ L/min	13 min 20 sec	4.8x faster
Acoustic focusing at 500 μ L/min	5 min 47 sec	11.0x faster
Acoustic focusing at 1,000 μ L/min	3 min 13 sec	19.7x faster

*A blood sample from an aplastic anemia individual with a PNH neutrophil population was analyzed on a conventional hydrodynamic focusing cytometer and on the Attune™ Acoustic Focusing Cytometer, each with a stop gate set on one million granulocyte events, and the time of acquisition was recorded.

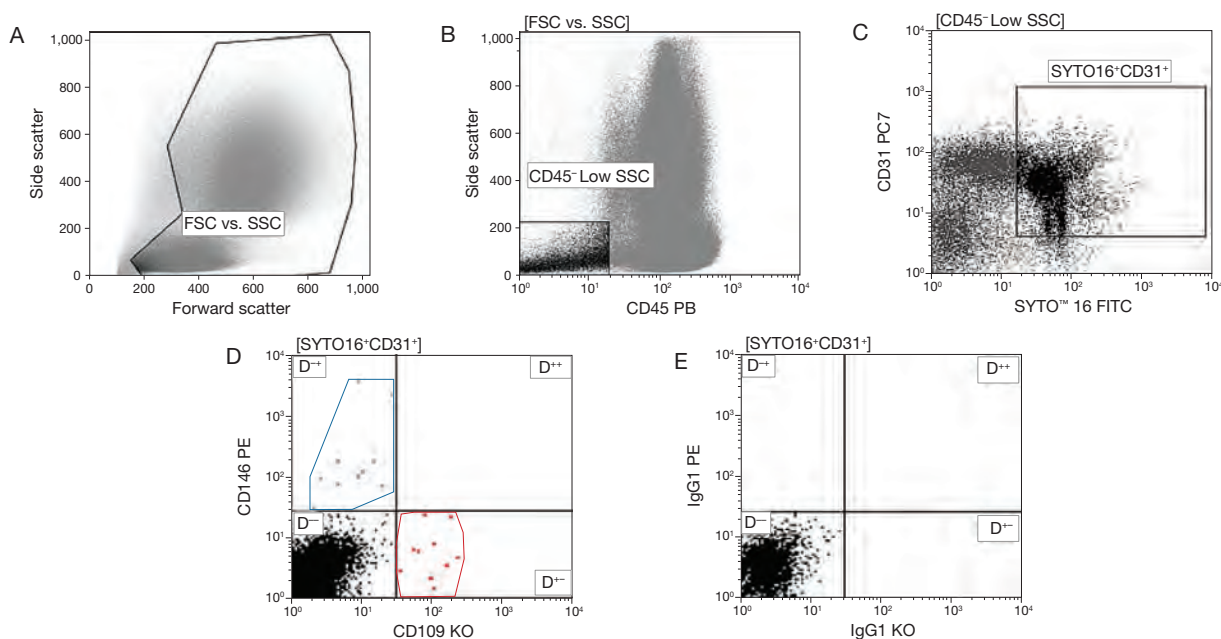


Figure 1. Gating strategy to detect circulating endothelial cells (CECs) expressing CD109 and CD146. The gating strategy includes exclusion of debris (A) and selection of CD45-negative (B), nucleated [positive for SYTO™ 16 stain, Cat. No. S7578] and CD31-positive (C) cells, followed by the identification of CECs as positive for CD109 (red) or CD146 (blue) (D). (E) Negative control. Reprinted with permission from Manusco P et al. (2014) *PLoS One* 9(12):e114713.

population of events from further analysis, is commonly referred to as a “dump channel”. Events typically excluded from analysis are dead and dying cells, cell aggregates and debris, and cells with unwanted markers or characteristics. Additionally, fluorescent-minus-one (FMO) controls—in which every fluorescent marker except one is used to determine the fluorescence contribution of all other markers to the detection channel for the excluded marker—are useful in determining points of separation between positive and negative populations.

To illustrate such a gating approach, a strategy for the detection of circulating endothelial cells (CECs) developed by Manusco and coworkers [5] is shown in Figure 1. CECs are vascular cells that have been shed from the vascular wall into the bloodstream. CECs and their progenitor cells are extremely rare in normal blood (0.01–0.0001% of peripheral mononuclear cells) but have been found to be elevated in various disease states, including cardiovascular disease and several cancers [6]. To detect CECs expressing CD109 or CD146 (two subpopulations enriched in the blood of cancer samples), the researchers used the cell-permeant SYTO™ 16 nucleic acid stain to discriminate between DNA-containing cells and cell debris, as well as a panel of fluorescent monoclonal antibody conjugates that included anti-CD45 (to exclude hematopoietic cells), anti-CD31 and anti-CD34 (endothelial cell markers), and anti-CD109 or anti-CD146 (markers expressed in the CECs of interest) antibodies. Figure 1D

shows the rare CD109⁺ (red) and CD146⁺ (blue) cell populations identified by combining compound gating with negative gating.

As a second example, Figure 2 shows two negative gating strategies designed to eliminate cell debris (using forward scatter vs. side scatter) and dead cells (using the SYTOX™ AADvanced™ Dead Cell Stain) during the detection of CECs with a panel of fluorescent anti-human CD antibodies. SYTOX™ AADvanced™ stain is a cell-impermeant nucleic acid dye for dead-cell detection that is compatible with excitation from the common 488 nm argon-ion laser. A detailed protocol for detecting human CECs using the Attune™ cytometer is provided at thermofisher.com/attuneappnotesbp71.

Another obstacle in any immunophenotyping experiment is the background fluorescence that arises from nonspecific antibody binding. Unlabeled normal mouse IgG antibody is commonly used to block Fc-binding receptors in samples prior to any staining protocols in order to reduce this nonspecific binding, decrease background fluorescence, and increase signal-to-noise ratios.

Detecting rare tumor cells in cancer studies

In cancer research, flow cytometry has been used to detect tumor cells by the presence or absence of specific cell-surface markers, typically in blood, bone marrow, and other fluids. The tumor cells of interest are often “buried” within a background of normal cells,

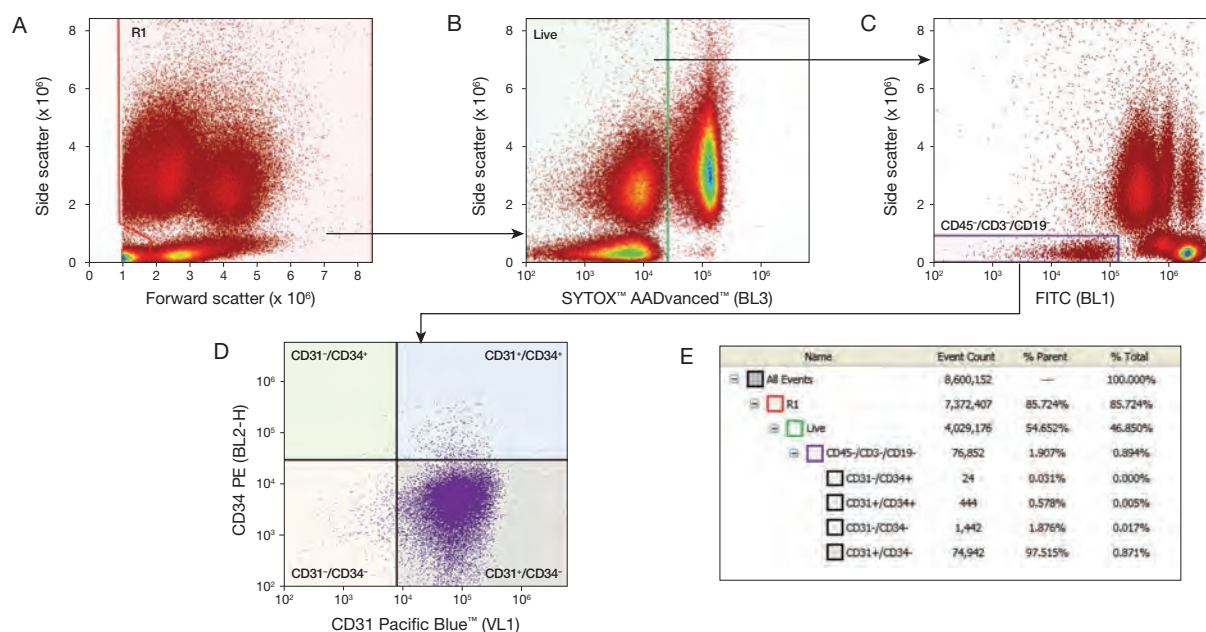


Figure 2. Gating to eliminate debris and dead cells for detection of circulating endothelial cells (CECs). (A) A density plot of forward scatter (FSC) vs. side scatter (SSC) shows both the threshold level and the R1 gate to remove debris. (B) Gated on R1 events, this density plot of SYTOX™ AADvanced™ stain (Cat. No. S10274) fluorescence (BL3) vs. side scatter shows the live cell gate, which eliminated dead cells. (C) Gated on live cells, this density plot of the FITC dump channel (BL1) vs. side scatter shows the gate on CD45⁻ CD3⁻ CD19⁻ cells. Since CECs are negative for all three of these markers, all positive cells can be eliminated from further analysis using only one fluorescence channel. (D) Gated on live CD45⁻ CD3⁻ CD19⁻ cells, CECs are identified as CD31⁺ CD34⁺ in the upper right-hand quadrant. (E) CECs are 0.578% of the parent CD45⁻ CD3⁻ CD19⁻ cells and 0.011% of the total live WBCs.

or may be extremely dilute [e.g., after detaching from a solid tumor and entering the bloodstream]. One of the early applications of rare-event detection was the analysis of minimal residual disease (MRD) in leukemia patients. MRD refers to the small number of residual cancer cells remaining in a subject during or after treatment, which may be undetectable by morphologic analysis. Using multicolor flow

cytometry, however, researchers have detected MRD in leukemia considered to be in remission by morphologic criteria. Figure 3 demonstrates the detection of a leukemia-associated immunophenotype (CD34⁺ CD13⁺ CD45^{WEAK} CD25⁺) in an acute myeloid leukemia (AML) sample after induction chemotherapy. In this study, the MRD represents only 0.003% of all nucleated peripheral blood cells [7]. →

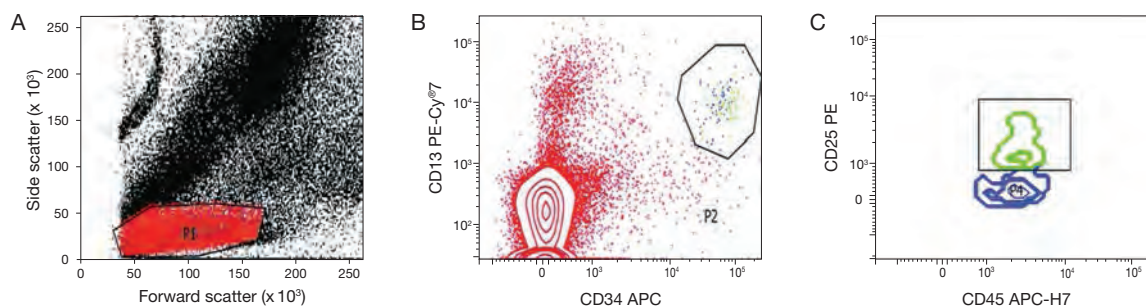


Figure 3. Flow cytometric detection of MRD after induction chemotherapy in the peripheral blood of an AML patient. In the scattergram (A), a gate (P1) is set around cells with low forward scatter (FSC) and side scatter (SSC), reflecting small to intermediate size and low granularity, respectively. In the blast gate (B), cells within P1 with high CD34 and high CD13 expression are selected away (P2) from CD34⁺ CD13⁺ cells (red dots), representing predominantly lymphocytes. Some CD34⁺ CD13⁺ cells are monocytes caught in P1. In the blast cell contour plot (C), MRD is detected within the CD34⁺ CD13⁺ gate based on the expression of CD25 and intermediate CD45 staining (green cluster). These cells with the patient's LAIP features (CD34⁺ CD13⁺ CD45^{WEAK} CD25⁺) account for 0.003% of all nucleated cells, a common denominator for MRD definition. The blue CD25⁻ cluster represents normal myeloid precursor cells (CD34⁺ CD13⁺ CD45^{WEAK} CD25⁻) caught in P2. Reprinted with permission from American Society of Hematology: Paietta E (2012) *Hematology Am Soc Hematol Educ Program* 2012:35–42.

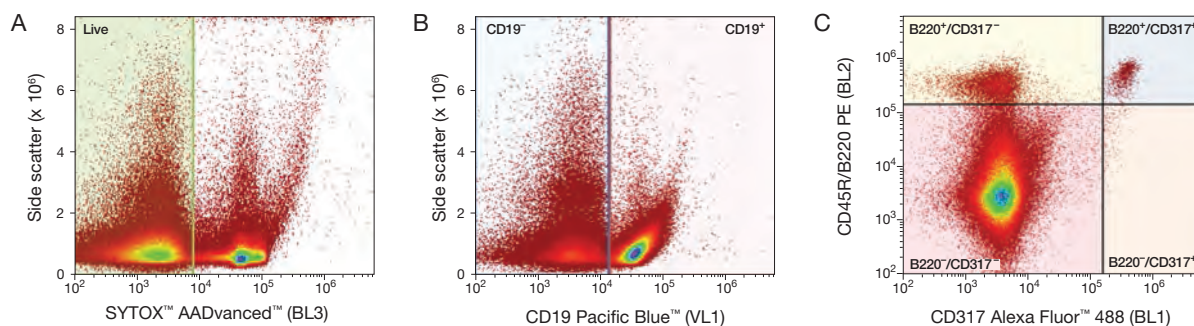


Figure 4. Mouse plasmacytoid dendritic cell (pDC) gating and analysis. (A) A gate was made on live cells using SYTOX™ AADvanced™ Dead Cell Stain (Cat. No. S10274; channel BL3, 640 nm longpass filter). (B) Live cells were then gated on CD19[−] cells (channel VL1, 450/40 nm bandpass (BP) filter). (C) A 2-parameter plot of CD45R/B220 vs. CD317 was used to detect pDCs (channel BL1, 530/30 nm BP filter; and channel BL2, 574/26 nm BP filter); pDCs were identified as dual B220⁺/CD317⁺ (upper right quadrant) and comprise 0.851% of live CD19[−] cells, which is 0.194% of total splenocytes. A collection rate of 500 μ L/min was used to acquire 1.3 million total cells; total acquisition time was 23 min, which is 3x faster than the same sample run on a traditional hydrodynamic focusing cytometer.

Circulating tumor cells (CTCs) are another active area of cancer research. CTCs have been detected in the blood of subjects with solid tumors, and their presence can be predictive of disease state and clinical outcome [8]. Flow cytometry has been used to analyze tumor metastasis to bone marrow and lymph node in preclinical models [9] and to detect rare tumor cells in human blood samples [10]. Today, flow cytometry is an essential tool for the detection of rare tumor cells in cancer research [1].

Acoustic cytometry for improved rare-event detection

The large number of cells required for rare-event detection can translate into very long acquisition times on a traditional hydrodynamic focusing flow cytometer. By comparison, acoustic focusing cytometry aligns cells using acoustic forces rather than hydrodynamic forces, delivering much higher throughput compared to traditional flow cytometry and enabling more cells to be analyzed in a shorter period of time (Table 2). Because there is minimal data variation regardless of sample-throughput rate, acoustic focusing cytometry is ideal for detecting rare-cell events as well as for analyzing dilute samples such as cerebrospinal fluid, in which low cell numbers necessitate large sample volumes.

The recently introduced Attune™ NxT Acoustic Focusing Cytometer achieves sample-throughput rates over 10 times faster than those of other cytometers (up to 1,000 μ L/min) and data acquisition speeds of 35,000 events/sec, enabling rapid detection of rare events with precision and accuracy and without aborting data. The Attune™ NxT cytometer retains all the acoustic focusing benefits of the first-generation Attune™ cytometer, while also providing additional lasers (up to 4 spatially separated lasers), more detection channels

(up to 14 emission channels plus forward and side scatter channels), and improved software that can manage the large data sets (up to 20 million events per run) generated during multiparameter analyses. Figure 4 shows a successful gating strategy for identifying mouse plasmacytoid dendritic cells (pDCs)—which are 0.194% of total splenocytes—using the Attune™ NxT cytometer.

Bring rare-event detection to your lab

Rare-event detection has become an essential tool for a host of applications, such as identification of antigen-specific cell populations, monitoring of hematological cancers, and detection of circulating tumor cells and endothelial cells. The success of rare-event cell detection is affected by many parameters, including sample quality, frequency of the cells of interest, sample preparation, specificity and expression levels of the chosen markers, and robustness and reproducibility of the assay. The next-generation Attune™ NxT Acoustic Focusing Cytometer provides a benchtop instrument with the performance and reliability that rare-cell detection requires. To request an in-lab demonstration, visit thermofisher.com/attunebp71. ■

References

1. Hedley BD, Keeney M [2013] *Int Jnl Lab Hem* 35:344–350.
2. Zimmerlin L, Donnenberg VS, Donnenberg AD [2011] *Methods Mol Biol* 699:251–273.
3. Gratama JW, Menéndez P, Kraan J et al. [2000] *J Immunol Methods* 239:13–23.
4. Allan AL, Keeney M [2010] *J Oncol* 426218.
5. Manusco P, Calleri A, Gregato G et al. [2014] *PLoS ONE* 9:e114713.
6. Boos CJ, Lip GY, Blann AD [2006] *J Am Coll Cardiol* 48:1538–1547.
7. Paietta E [2012] *Hematology Am Soc Hematol Educ Program* 2012:35–42.
8. Yu M, Stott S, Toner M et al. [2011] *J Cell Biol* 192:373–382.
9. Goodale D, Phay C, Postenka CO et al. [2009] *Cytometry A* 75:344–355.
10. Watanabe M, Uehara Y, Yamashita N et al. [2014] *Cytometry A* 85:206–213.

The next generation in acoustic focusing cytometry

The Attune™ NxT Acoustic Focusing Cytometer.

The Attune™ NxT Acoustic Focusing Cytometer is a benchtop analyzer (Figure 1) that uses acoustic focusing—a revolutionary technology that precisely aligns cells using ultrasonic waves prior to interrogation with one or more lasers. This technology enables multicolor flow cytometric analysis with significantly greater collection rates and an improved ability to detect rare events without excess sample manipulation. The Attune™ NxT system offers:

- Unique modular design—one-day field-upgradable system with configurations for 1–4 lasers and up to 14 emission channels
- Fast detection speeds—short acquisition times without loss of data quality enable applications such as rare-event detection (see page 14) and use of no-lyse/no-wash techniques (see page 28)
- Distinctive acquisition and analysis software—intuitive and powerful for users of all experience levels
- Convenient size—complete setup fits on your benchtop

Multicolor analysis in a modular design

With up to 4 lasers and 14 emission channels for multiparameter analysis, the Attune™ NxT Acoustic Focusing Cytometer was designed as a modular system to fit most experimental needs and lab budgets (Table 1). The Attune™ NxT cytometer can be configured to accommodate most common fluorophores used in flow cytometry, as well as to match the panels you are currently running. For example, with the optional violet and yellow lasers (in addition to the standard blue laser), the Attune™ NxT cytometer can be used to simultaneously detect multiple fluorescent proteins (see page 23).

Whether you configure your system now or upgrade later, the Attune™ NxT Acoustic Focusing Cytometer can grow with you and your research needs. To find out more and request an in-lab demonstration, visit thermofisher.com/attunebp71. ■



Figure 1. Attune™ NxT Acoustic Focusing Cytometer with optional Attune™ NxT Autosampler, for processing up to 384 samples.

Table 1. Specifications for the Attune™ NxT cytometer.

Feature	Attune™ NxT Acoustic Focusing Cytometer
Size, weight	40 x 58 x 43 cm (16 x 23 x 17 in), 29 kg (64 lb)
Electrical	100–240 VAC, 50/60 Hz, <150 W
Excitation	<p>Up to 4 lasers: Violet (405 nm, 50 mW), blue (488 nm, 50 mW), yellow (561 nm, 50 mW), red (637 nm, 100 mW)</p> <p>Laser profile: Flat-top laser requiring minimal alignment</p> <p>Flow cell: Quartz cuvette gel-coupled to 1.2 NA collection lens</p>
Emission	<p>Forward scatter: Photodiode detector with 488/10 nm bandpass filter</p> <p>Side scatter: PMT with 488/10 nm bandpass filter</p> <p>Emission filters: User-changeable, keyed filters</p>
Fluidics	<p>Sample rate: 12.5–1,000 µL/min</p> <p>Sample analysis volume: 20 µL–4 mL</p> <p>Sample tube size: 17 x 100 mm to 8.5 x 45 mm</p> <p>Sample delivery: Positive-displacement syringe pump</p> <p>Fluid storage: All fluids stored within instrument with active fluid level sensing (optional external tank available)</p>
Performance	<p>Data acquisition rate: Up to 35,000 events/sec</p> <p>Maximum event file: 20 million</p> <p>Particle size range: 0.5–50 µm</p> <p>Automated maintenance: ≤15 min startup and shutdown</p>

Product	No. of lasers	No. of emission channels *	Cat. No.
Attune™ NxT Acoustic Focusing Cytometer—Blue Laser	1	4	A24864
Attune™ NxT Acoustic Focusing Cytometer—Blue/Red Lasers	2	7	A24863
Attune™ NxT Acoustic Focusing Cytometer—Blue/Violet Lasers	2	8	A24862
Attune™ NxT Acoustic Focusing Cytometer—Blue/Yellow Lasers	2	7	A24861
Attune™ NxT Acoustic Focusing Cytometer—Blue/Red/Violet Lasers	3	11	A24860
Attune™ NxT Acoustic Focusing Cytometer—Blue/Violet/Yellow Lasers	3	11	A24859
Attune™ NxT Acoustic Focusing Cytometer—Blue/Red/Violet/Yellow Lasers	4	14	A24858

*Number of different emission channels, in addition to the forward scatter (FSC) and side scatter (SSC) detection channels.

Flow cytometry panel design: The basics

Multiplex flow cytometry experiments need the right combination of fluorophores.

Advances in both flow cytometry reagents and instrumentation allow researchers to run increasingly complex multicolor experiments. The advantages of multiparameter flow cytometry include the ability to perform single-cell interrogation with multiple markers, to correlate cell data using multiple analytes, and ultimately to more accurately define cell populations (Figure 1). Additionally, multiparameter experiments can improve efficiency by requiring fewer samples and smaller sample volumes and by increasing sample throughput. Increasing the number of colors and antigens detected, however, increases the complexity of the experimental design, requiring significantly higher attention to optimization, controls, and other details [1].

One of the biggest challenges in multiparameter flow cytometry is selecting the right combination of fluorophores and antibody conjugates so that the need for compensation and spillover adjustments is kept to a minimum while the quality and accuracy of the data are not compromised. There are some excellent resources available for the beginner, including the Molecular Probes™ webinar

“Multicolor Flow Cytometry Panel Design” by Dr. Holden Maecker of Stanford University. Additional publications on this topic are available [2–4].

When designing a multicolor flow cytometry panel, there are several key points to consider:

- Know the configuration of the instrument being used (laser and filters) before you begin.
- Use a tool like the Molecular Probes™ Fluorescence SpectraViewer to visualize the spectral overlap of fluorophores.
- Titrate and optimize each antibody; building the right panel is an iterative process.
- Use bright fluorophore labels on antibodies for low-abundance antigens and dim fluorophore labels on antibodies for highly expressed antigens.
- Use fluorophores that are spectrally similar for different cell subpopulations that will be gated and analyzed separately.
- Include a cell viability dye in the panel to exclude dead cells and debris from the data.

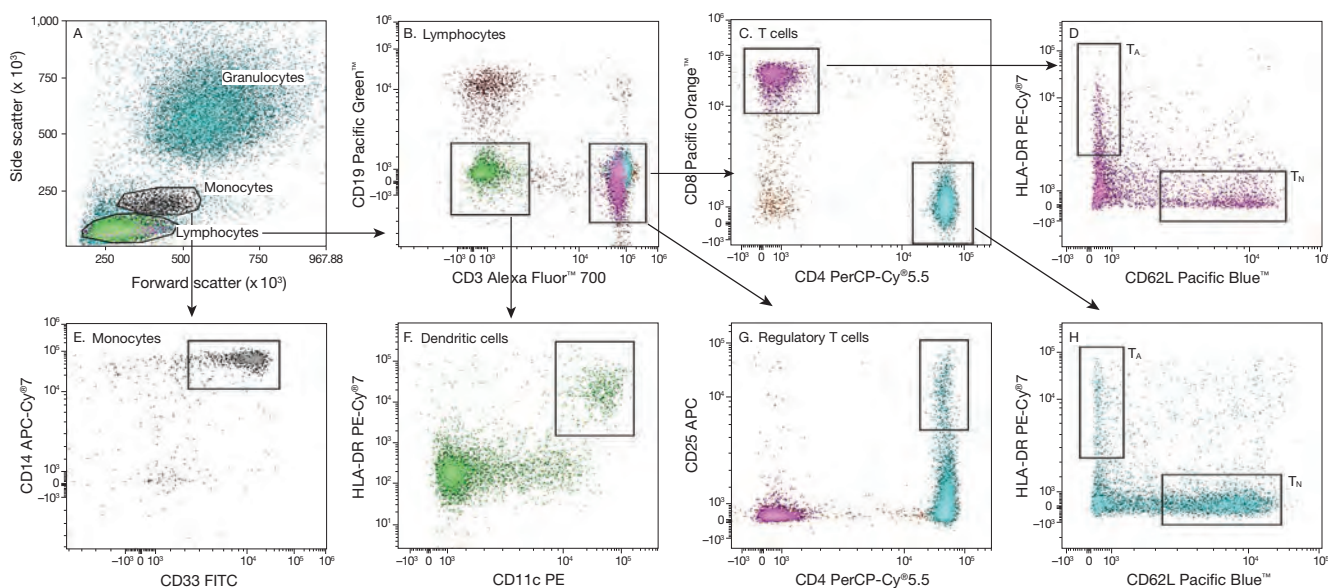


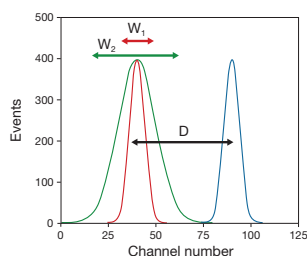
Figure 1. Ten-parameter immunophenotyping of human peripheral blood mononuclear cells (PBMCs) with the Attune™ NxT Acoustic Focusing Cytometer. Lymphocytes and monocytes were gated based on forward- and side-scatter profiles (A). Within the lymphocyte gate, T cells can be isolated based on their expression of CD3 (B), and further subdivided into CD4⁺ and CD8⁺ subpopulations (C). In addition, regulatory T cells express CD4 and CD25 (G) and are important mediators of dominant peripheral tolerance. CD62L identifies naive CD4⁺ and CD8⁺ T cells (T_N), whereas HLA-DR is expressed by activated T cells (T_A) (D, H). Conventional dendritic cells found in peripheral blood are generally negative for T and B cell lineage markers and co-express the integrin CD11c and HLA-DR (F). Monocytes are located just above lymphocytes in the scatter profile (A), and express both CD14 and CD33 (E).

Determining fluorophore brightness

In flow cytometry, fluorophore brightness is a function not only of the quantum yield and extinction coefficient of the fluorophore itself, but also of the effects of background contributions. Background fluorescence—e.g., from nonspecific staining, cellular autofluorescence, and instrument noise—can affect the ability to resolve the fluorescence of the antibody conjugate-stained cell population (positive) from that of the unstained cell population (negative).

The signal-to-noise ratio (S/N) is one measure of the sensitivity of an assay and its ability to detect differences between stained and unstained populations. To calculate a simple S/N, divide the median fluorescence intensity (MFI) of the positive cells by that of the negative cells (Figure 2).

However, the relative brightness of a fluorophore-conjugated antibody is determined not only by the intensity difference between stained and unstained cells, but also by the intensity distribution spread of the unstained cell population. Proposed by Maecker et al. [2], the Stain Index (SI) takes these two parameters into account (Figure 2). The SI can be useful for comparing histograms of cell populations stained with different fluorescent conjugates of the same antibody (Table 1, Figure 3).



Stain Index = D/W

Where:

D is the difference between positive and negative peak medians.

W is the spread of the negative peak and is equal to 2 x rSD.

rSD is the robust standard deviation.

Signal-to-noise ratio = MFI (positive cells) / MFI (negative cells)

Where:

MFI is the median fluorescence intensity.

Figure 2. Comparison of Stain Index (SI) and signal-to-noise ratio (S/N). An illustration of two fluorophores with the same S/N but different SI due to different widths of the negative peak (narrow W_1 vs. wide W_2). Because the width of the negative peak affects the separation of the positive and negative signals, SI is the preferred statistic when comparing fluorophore brightness.

Table 1. Staining Index for different fluorophore conjugates of an anti-CD4 antibody (clone 53.5).

Brightness	Fluorophore component of conjugate (Conjugate Cat. No.)	Ex max*	Em max*	Laser line	BP Em filter†	Stain Index
High	APC (MHCD0405)	645	660	633	660/20	200.31
	PE (MHCD0404)	496, 565	575	488	585/42	158.46
	APC-Cy5.5 (MHCD0419)	650	690	633	710/50	108.97
	PE-Cy5.5 (MHCD0418)	496, 565	690	488	695/40	105.91
	Alexa Fluor™ 488 dye (MHCD0420)	495	519	488	525/50	91.72
Medium	PE-Alexa Fluor™ 610 dye (MHCD0422)	488	628	488	620/10	70.71
	FITC dye (MHCD0401)	493	525	488	525/50	56.40
	PE-Cy7 (MHCD0412)	496, 565	774	488	780/60	53.70
	PE-Alexa Fluor™ 700 dye (MHCD0424)	496, 565	723	488	720/30	52.45
	TRI-COLOR™ dye (PE-Cy5) (MHCD0406)	496, 565	670	488	695/40	50.31
	PE-Texas Red™ dye (MHCD0417)	496, 565	613	488	695/40	40.85
	Qdot™ 605 nanocrystal (Q10008)	350	605	405	605/20	35.17
	APC-Alexa Fluor™ 750 dye (MHCD0427)	645	775	633	780/60	31.91
	Alexa Fluor™ 700 dye (MHCD0429)	696	719	633	710/50	24.85
	Qdot™ 655 nanocrystal (Q10007)	350	655	405	655/20	20.62
Low	Qdot™ 705 nanocrystal (Q10060)	350	720	405	720/20	18.38
	Pacific Blue™ dye (MHCD0428)	410	455	405	450/50	14.61
	Alexa Fluor™ 405 dye (MHCD0426)	401	421	405	450/50	10.01
	PerCP (MHCD0431)	482	675	488	695/40	8.75
	Pacific Orange™ dye (MHCD0430)	400	551	405	585/42	6.06

*Approximate fluorescence excitation (Ex) and emission (Em) maxima for conjugates, in nm. †BP Em filter = bandpass emission filter, in nm. Staining Index was determined on the BD™ LSR II Flow Cytometer with FACSDiva™ version 6.1 software.

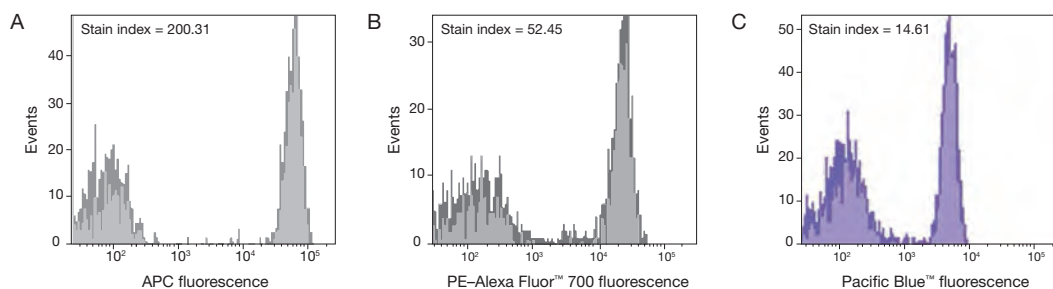


Figure 3. Representative histograms for cells stained with anti-CD4 antibody conjugates. Ammonium chloride-lysed human whole blood was used to evaluate the performance of 20 different mouse anti-human CD4 antibody direct conjugates (see Table 1). Each conjugate was titrated and optimized to produce a maximum signal-to-noise ratio. Cells were analyzed on a BD™ LSR II Flow Cytometer with FACSDiva™ version 6.1 software. Histograms represent 10,000 cells collected in a lymphocyte gate: **(A)** high brightness from anti-CD4 antibody, APC conjugate; **(B)** medium brightness from anti-CD4 antibody, PE-Alexa Fluor™ 700 conjugate; **(C)** low brightness from anti-CD4 antibody, Pacific Blue™ conjugate. The Stain Index (SI) for each conjugate is listed in the left corner of the plot.

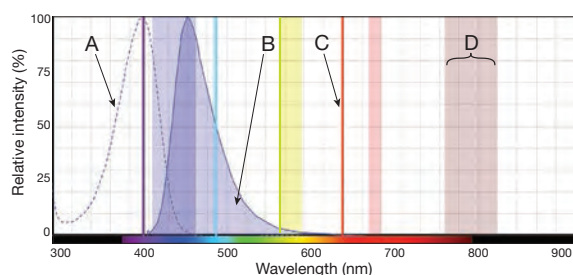


Figure 4. Overview of Molecular Probes™ SpectraViewer components. (A) Excitation spectrum and (B) emission spectrum for the same fluorophore. (C) Laser excitation wavelength. (D) Bandpass emission filter wavelengths.

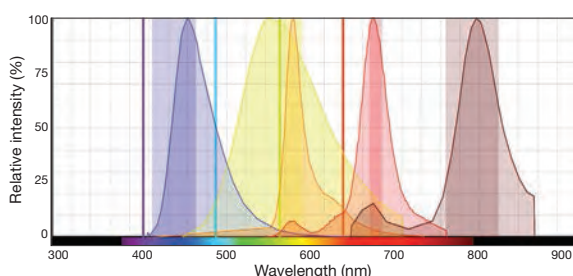


Figure 5. Five-color panel depicted on the Molecular Probes™ SpectraViewer. Emission curves for Pacific Blue™ dye (purple) excited by the 405 nm laser, LIVE/DEAD™ Fixable Yellow stain (yellow) excited by the 405 nm laser, R-phycoerythrin (PE, orange) excited by the 488 nm laser, Alexa Fluor™ 647-PE (red) excited by the 561 nm laser, and Alexa Fluor™ 750-allophycocyanin (brown) excited by the 633 nm laser. Lasers shown are 405 nm (violet), 488 nm (blue), 561 nm (yellow), and 633 nm (red).

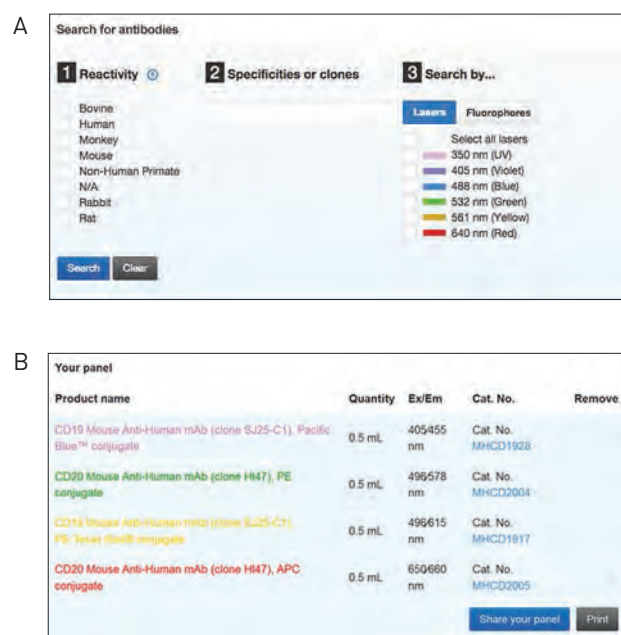


Figure 6. Screenshots from the new Panel Design tool.

Table 2. SpectraViewer spillover table for five fluorophores (Figure 5) with emission filter configurations found on the Attune™ NxT cytometer.

Fluorophore	Bandpass [BP] emission filter (nm)			
	440/50	574/26	670/14	780/60
Pacific Blue™ dye	48.2%	0.9%	0.0%	0.0%
LIVE/DEAD™ Fixable Yellow stain	0.2%	20.3%	2.2%	0.0%
PE (R-phycoerythrin)	0.0%	53.7%	1.2%	0.0%
Alexa Fluor™ 647-PE	0.0%	3.3%	28.9%	0.1%
Alexa Fluor™ 750-allophycocyanin	0.0%	0.0%	2.9%	66.1%

Percentages represent the relative fluorescence signal detected with the indicated emission filters (independent of excitation light source). The 574/26 nm BP filter collects 20.3% and 53.7% of the LIVE/DEAD™ Fixable Yellow stain and PE fluorescence, respectively. However, there should be no actual spillover because the LIVE/DEAD™ stain is excited at 405 nm but not 488 nm, and PE is excited at 488 nm but not 405 nm; i.e., they will be excited using different lasers.

Online tools: Fluorescence SpectraViewer and Panel Design

The Molecular Probes™ Fluorescence SpectraViewer is an online tool that displays the excitation and emission spectra for fluorescent dyes and proteins, facilitating selection of appropriate dyes for your multicolor experiment. You can enter your instrument laser and filter configuration (Figure 4), then select the fluorophores under consideration. Figure 5 shows an example of a five-color panel. An additional feature of the SpectraViewer is the spillover table function, which shows fluorescence overlap (or spillover) for each dye in each channel (Table 2). You can find the Fluorescence SpectraViewer at thermofisher.com/spectraviewer.

Our new Panel Design tool can help you choose fluorescent antibody conjugates for your flow cytometry panel in four easy steps: 1) go to thermofisher.com/flowpanel, 2) pick the antibody species reactivity you want to include in your search, 3) select up to 14 targets of interest (choices include viability dyes), and 4) choose the lasers or fluorophores you want to view (Figure 6A). The available antibodies and dyes for your targets will be displayed on a tab for each laser, or you can scroll down the page to find the laser tables. The number of products available will be displayed in each cell; simply click on the number and select the product you want from the list in the pop-up window. Your panel choices will be displayed at the top of the table (Figure 6B). When you are finished choosing products, either print your list or share it via email. Find these online tools and the panel design webinars at thermofisher.com/flowresourcesbp71. ■

References

1. Perfetto SP, Chattopadhyay PK, Roederer M (2004) *Nat Rev Immunol* 4:648–655.
2. Maecker HT, Frey T, Nomura LE, Trotter J (2004) *Cytometry A* 62:169–173.
3. Maecker HT, Trotter J (2006) *Cytometry A* 69:1037–1042.
4. Mahnke YD, Roederer M (2007) *Clin Lab Med* 27:469–485.

Keep pace with the surge in fluorescent protein choices

Multicolor detection of fluorescent protein expression with the Attune™ NxT Acoustic Focusing Cytometer.

Since the discovery of Green Fluorescent Protein (GFP) in the 1960s, the use of fluorescent proteins (FPs) in biological studies has exploded. In its role as a reporter, GFP has added a new dimension to the analysis of protein function and localization, allowing real-time examination in live cells and processes that previously had been observed only through immunocytochemical “snapshots” in fixed specimens.

Fluorescent proteins are widely used to investigate gene expression, as well as protein localization, translocation, and trafficking within live cells. More advanced techniques include assessment of protein–protein interactions and spatial relation of proteins in live cells with fluorescence resonance energy transfer (FRET) techniques and fluorescence lifetime imaging microscopy (FLIM). In addition, far red–emitting FPs, which exhibit emissions beyond typical autofluorescence wavelengths, have proven useful for imaging of tissues. Even more recently, FPs have been used to assess intracellular topology in live cells using super-resolution localization imaging.

The quest for new FPs with unique excitation and emission profiles has been the focus of many distinguished laboratories, and mutation and evolution of such proteins has led to the creation of variants including the “fruit” FPs (e.g., tdTomato, mStrawberry,

mCherry, mPlum, and mRaspberry), specialized FPs such as the fluorescent timer protein Kusabira Green Orange, long–Stokes shift (LSS) fluorescent proteins such as LSS–mKate2, and photoswitchable FPs (e.g., Dendra2 and mEos2).

Versatile tools for flow cytometry

The use of FPs became popularized in the field of flow cytometry in the 1990s after mutation of wild-type GFP resulted in a variant optimally excited by the 488 nm argon-ion laser common to most flow cytometers [1]. Early studies using FPs in flow cytometry include the quantitative detection and monitoring of gene expression in yeast [2], bacteria [3], and eukaryotic cells [4]. Today there are over 70 FPs available, of which 56 are commonly used in flow cytometry and exhibit excitation wavelengths between 355 nm and above 600 nm (Table 1). Flow cytometrists have taken advantage of this large set of choices—combined with the increased availability of alternate excitation sources such as the 405 nm, 532 nm, and 561 nm lasers—by developing multiparameter flow cytometry assays. These assays are designed to analyze cells expressing several different FPs [5,6], as well as FP-expressing cells that have also been labeled with fluorescent antibodies and functional probes [7,8].



Table 1. Spectral characteristics of fluorescent proteins commonly used in flow cytometry.

Fluorescent protein	Excitation max (nm)	Emission max (nm)	Channel on the Attune™ NxT Acoustic Focusing Cytometer
Azurite, TagBFP, mTagBFP, mTagBFP2, Cerulean, ECFP, TagCFP, AmCyan	383, 400, 400, 400, 433, 439, 458, 458	450, 456, 456, 456, 475, 476, 480, 489	VL1 (440/50)
T-Sapphire	399	511	VL2 (512/25)
LSS–mKate1, LSS–mKate2	463, 460	624, 605	VL3 (603/48)
TurboGFP, EGFP, TagGFP, Emerald GFP	482, 483, 484, 487	502, 506, 507, 509	BL1 (530/30) (510/10)*
TagYFP, TurboYFP, EYFP, Topaz, Venus, Citrine	508, 508, 514, 514, 515, 517	524, 524, 527, 527, 528, 529	BL1 (530/30) (510/10)* or BL2 (574/26) (540/30)*
mKOm, mOrange, mOrange2, Kusabira Green Orange, E2 Orange	548, 548, 549, 548, 540	559, 562, 565, 561, 561	YL1 (585/16)
DsRed, DsRed2, DsRed-Express, tdTomato, TagRFP, mStrawberry, mCherry, mKate, mKate2, TurboFP635 (Katushka)	553, 553, 553, 554, 555, 574, 587, 588, 588, 588	583, 583, 584, 581, 584, 596, 610, 635, 633, 635	YL2 (620/15) (615/25)*
mPlum, HcRed, mRaspberry, mNeptune, E2Crimson	590, 592, 598, 599, 611	649, 645, 625, 649, 646	YL3 (695/40)

* Bandpass emission filter when using the fluorescent protein filter kit (optional, Cat. No. 100022775)

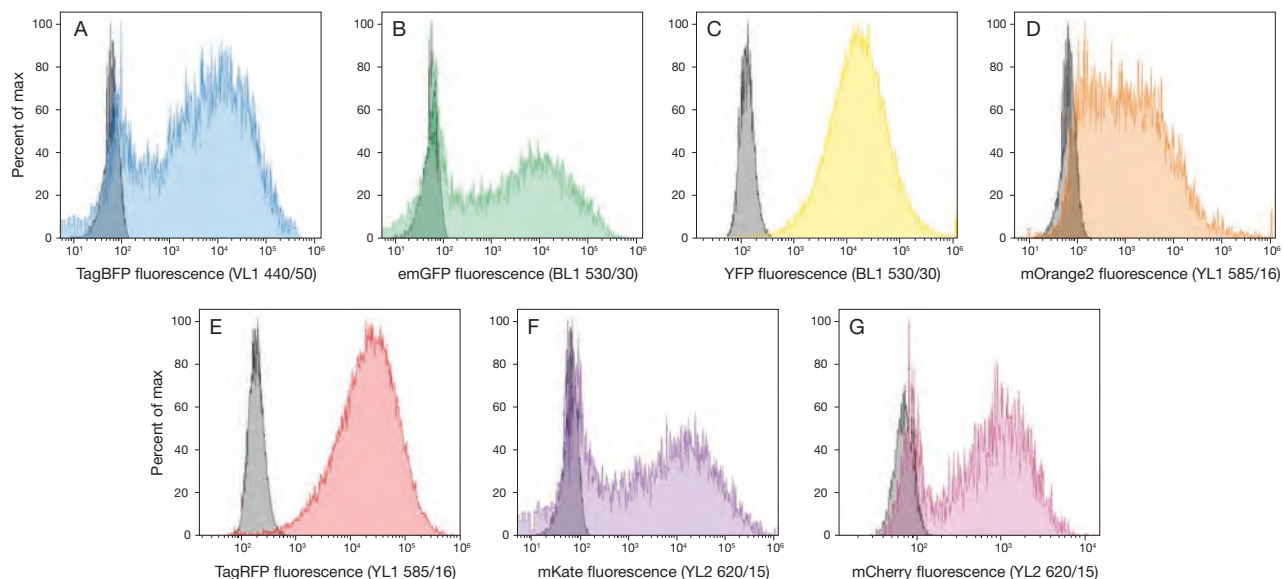


Figure 1. Detection of a palette of fluorescent proteins using the Attune™ NxT Acoustic Focusing Cytometer. 293FT cells or U2OS cells were transfected or transduced with plasmid or viral constructs expressing different fluorescent proteins. Samples were acquired on the Attune™ NxT cytometer at a flow rate of 100 μ L/min using 405 nm, 488 nm, or 561 nm excitation sources. **(A)** Blue Fluorescent Protein (TagBFP) fluorescence was collected in the VL1 channel using a 440/50 bandpass (BP) filter; **(B)** Emerald GFP (emGFP) fluorescence and **(C)** Yellow Fluorescent Protein (YFP, Venus variant) fluorescence (in cells transduced with the Premo™ Halide Sensor) were collected in the BL1 channel using a 530/30 BP filter; **(D)** Orange Fluorescent Protein (mOrange2) fluorescence and **(E)** Red Fluorescent Protein (TagRFP) fluorescence were collected in the YL1 channel using a 585/16 BP filter; **(F)** mKate fluorescence and **(G)** mCherry fluorescence were collected in the YL2 channel using a 620/15 BP filter. Control cells that do not express fluorescent protein are shown in each histogram overlay (gray peaks). TagBFP, mOrange2, TagRFP, YFP, and mCherry were expressed from the CMV promoter, and emGFP and mKate were expressed from the EF-1 α promoter. YFP and RFP constructs were delivered to U2OS cells using the BacMam 2.0 transduction system, whereas TagBFP, emGFP, mKate, and mOrange2 constructs were transfected into 293FT cells using Lipofectamine™ 3000 reagent. The mCherry construct was transduced into U2OS cells using an adenovirus delivery system.

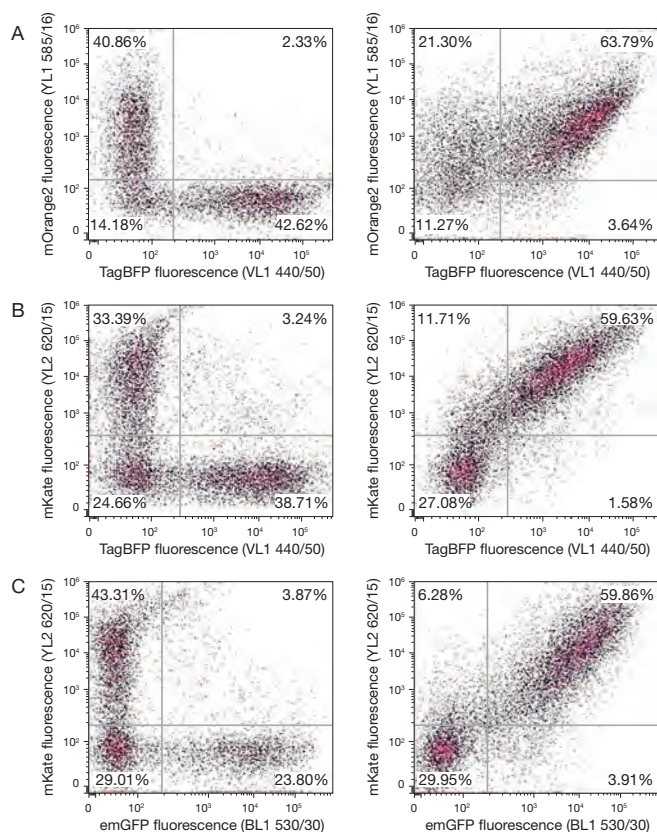


Figure 2. Detection of multiple FPs expressed in the same cell. Plasmid constructs were transfected alone (left panels) or simultaneously (right panels) in a 1:1 (w/w) mix into 293FT cells using Lipofectamine™ 3000 reagent. Transfected cells were grown for 48 hr prior to harvest and analysis by flow cytometry. Samples were acquired using an Attune™ NxT Acoustic Focusing Cytometer at a flow rate of 100 μ L/min, and a minimum of 15,000 events were collected for each sample. **(A)** Plasmids encode the Blue Fluorescent Protein (TagBFP) or Orange Fluorescent Protein (mOrange2) under control of the CMV promoter. The 405 nm and 561 nm lasers were used for excitation of TagBFP and mOrange2, respectively. TagBFP fluorescence was detected in the VL1 channel using a 440/50 bandpass (BP) filter, and mOrange2 fluorescence was detected in the YL1 channel using a 585/16 BP filter. **(B)** Plasmids encode TagBFP under control of the CMV promoter or the mKate Fluorescent Protein (mKate) under control of the EF-1 α promoter. The 405 nm and 561 nm lasers were used for excitation of TagBFP and mKate, respectively. TagBFP fluorescence was detected in the VL1 channel using a 440/50 BP filter, and mKate fluorescence was detected in the YL2 channel using a 620/15 BP filter. **(C)** Plasmids encode the Emerald Green Fluorescent Protein (emGFP) or mKate under control of the EF-1 α promoter. The 488 nm and 561 nm lasers were used for excitation of emGFP and mKate, respectively. emGFP fluorescence was detected in the BL1 channel using a 530/30 BP filter, and mKate fluorescence was detected in the YL2 channel using a 620/15 BP filter. All major cell populations are detected: cells expressing one of the FPs, both FPs, and neither FP (percentages are indicated on the plots). Cells expressing the fluorescent proteins are easily distinguished from non-expressing cells.

Detecting multiple FPs using the Attune™ NxT Acoustic Focusing Cytometer

With the option to be configured with up to 4 lasers and 16 detection channels (14 colors and 2 scatter channels), the Attune™ NxT Acoustic Focusing Cytometer is ideally suited for the detection of multiple FPs. The Attune™ NxT instrument has a modular design with a 488 nm laser for excitation of the most commonly used FP (EGFP) and its variants (emGFP, TurboGFP), and can be upgraded to include optional laser lines including 405 nm, 561 nm, and 637 nm lasers. The 561 nm laser is particularly useful for exciting the orange- and red-fluorescent protein variants: mCherry, the popular monomeric red-fluorescent protein with superior brightness and photostability [9]; mKate, known for its fast maturation rate as well as its high pH stability and photostability [10]; and mOrange2, a bright monomeric orange-fluorescent protein. The 405 nm laser can be used to excite FPs such as TagBFP [11], the bright blue-fluorescent mutant created from site-specific and random mutagenesis of TagRFP, or others including Azurite and T-Sapphire. Figure 1 shows detection of TagBFP, emGFP, YFP, mOrange2, TagRFP, mKate, and mCherry using the Attune™ NxT Acoustic Focusing Cytometer.

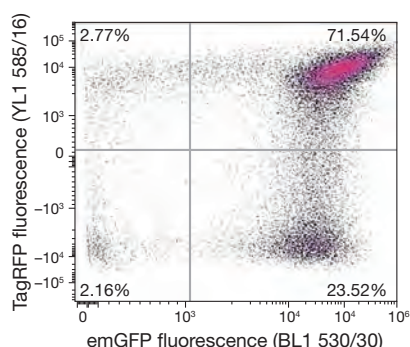


Figure 3. Live-cell detection with CellLight™ reagents. Baculovirus constructs encoding Emerald GFP (emGFP) or Red Fluorescent Protein (TagRFP) under control of the CMV promoter were co-transduced into U2OS cells using the BacMam 2.0 delivery system. Samples were acquired using a four-laser Attune™ NxT Acoustic Focusing Cytometer equipped with 405 nm, 488 nm, 561 nm, and 637 nm lasers. emGFP fluorescence was collected in the BL1 channel using a 530/30 bandpass (BP) filter, and TagRFP fluorescence was detected in the YL1 channel using a 585/16 BP filter. As expected, the majority of cells in the sample are co-positive for both FPs (emGFP⁺/TagRFP⁺, 71.54%). There are two minor populations of cells that only express one FP: emGFP⁺ TagRFP⁻ cells are 23.52% of the population and emGFP⁻ TagRFP⁺ cells are 2.77% of the population. Only a small number of cells do not express either protein (2.16%).

Simultaneous detection of paired FPs expressed in the same cell is shown in Figure 2, demonstrating clear separation of cells expressing one of the FPs, both FPs, or neither FP. For no-hassle labeling of specific organelles in live cells, CellLight™ ready-to-use constructs express fluorescent fusion proteins targeted to specific intracellular structures. With these reagents, the FP is introduced using a simple transduction step that doesn't require molecular biology techniques to carry out—they work like cell stains and can be detected easily using flow cytometry (Figure 3).

More resources for your fluorescent protein studies

Get the most out of your FP experiments. Visit our Flow Cytometry Resource Center at thermofisher.com/flowresourcesbp71 for useful tutorials, webinars, application notes, fluorophore guides, and more information on reagents and instrumentation for flow cytometry. ■

References

- Ropp JD, Donahue CJ, Wolfgang-Kimball D et al. (1995) *Cytometry* 21:309–317.
- Atkins D, Izant JG (1995) *Curr Genet* 28:585–588.
- Kremer L, Baulard A, Estaquier J et al. (1995) *Mol Microbiol* 17:913–922.
- Anderson MT, Tjioe IM, Lorincz MC et al. (1996) *Proc Natl Acad Sci U S A* 93:8508–8511.
- Hawley TS, Telford WG, Ramezani A (2001) *Biotechniques* 30:1028–1034.
- Hawley TS, Telford WG, Hawley RG (2001) *Stem Cells* 19:118–124.
- Gundry RL, Riordon DR, Tarasova Y (2012) *Mol Cell Proteomics* 11:303–316.
- Yang N, Huang B, Tsinkalovsky O et al. (2014) *Cancer Cell Int* 14:541–549.
- Shaner NC, Steinbach PA, Tsien RY (2005) *Nat Methods* 2:905–909.
- Shcherbo D, Merzlyak EM, Chepurnykh TV et al. (2007) *Nat Methods* 4:741–746.
- Subach OM, Gundorov IS, Yoshimura M et al. (2008) *Chem Biol* 15:1116–1124.

Product	Quantity	Cat. No.
Attune™ NxT Acoustic Focusing Cytometer—Blue/Red/Violet/Yellow Lasers	1 each	A24858
Attune™ NxT Fluorescent Protein Filter Kit	1 kit	100022775
Attune™ Performance Tracking Beads	3 mL	4449754
Attune™ Focusing Fluid (1X)	10 L	A24904
CellLight™ Plasma Membrane-RFP, BacMam 2.0	1 mL	C10608
CellLight™ Nucleus-RFP, BacMam 2.0	1 mL	C10603
CellLight™ Nucleus-GFP, BacMam 2.0	1 mL	C10602
GeneArt™ CRISPR Nuclease Vector with OFP Reporter Kit (with competent cells)	10 reactions	A21178
Lipofectamine™ 3000 Transfection Reagent	0.1 mL	L3000-001
Premo™ Halide Sensor	1 kit	P10229
293FT Cell Line	3 x 10 ⁶ cells	R700-07

Minimize—even eliminate—color compensation

No-compensation immunophenotyping using a four-laser flow cytometer.

With the option to be configured with up to 4 lasers and 14 colors for multi-parameter analysis, the Attune™ NxT Acoustic Focusing Cytometer was envisioned as a modular system to fit most experimental design needs and lab budgets. The novel design of the optical path helps ensure precise fixed alignment of 4 spatially separated lasers onto the sample stream, enabling consistency in data over time along with superior performance and reliability. And for the researcher who prefers to avoid color compensation, the 14 colors spread across the 4 independent laser lines allow popular dye combinations to be used with minimal or no compensation.

Spillover and compensation defined

Spillover occurs when the emission spectrum of a given fluorophore is detected in a detector meant to identify signal from another fluorophore (Figure 1). In order to appropriately visualize flow cytometry data, spillover needs to be corrected for by a process called compensation. Compensation is a way to mathematically subtract the overlap of fluorescence emission colors that occurs with multilabeled samples in flow cytometry. For example, even though the emission peaks of fluorescein (FITC; emission maximum ~525 nm) and R-phycoerythrin (PE; emission maximum ~575 nm) are well separated, the emission spectra of these two dyes overlap significantly (Figure 1).

During data acquisition on a flow cytometer equipped with a single blue (488 nm) laser, optical filters are used to direct the FITC emissions to the FITC detector and PE emissions to the PE detector. But because of their spectral overlap, some FITC emission light passes through the PE filter, which can result in a FITC-labeled target being counted in the PE detection channel. When this happens, software algorithms utilize data

collected from single-color stained controls to estimate the FITC signal collected by the PE detector and subtract it from the data—a process called color compensation. Appropriate compensation, however, not only requires extra controls and time but is also prone to artifacts and errors.

Uncouple the excitation and detection of multiple dyes

Compensation is not simple, requiring runs of positive and negative, color-matched controls in conjunction with careful monitoring of background fluorescence. The Attune™ NxT cytometer can be configured with up to 4 spatially separated lasers (see page 19), giving you the flexibility to choose dyes and detection channels that are well separated spectrally and do not have significant overlap (e.g., Table 1).

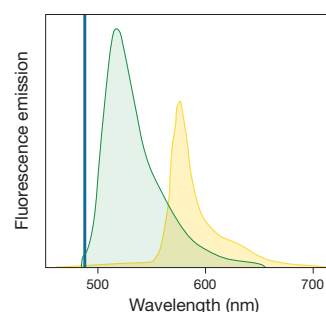


Figure 1. Spectra of fluorescein and R-phycoerythrin emission, demonstrating spectral overlap. Emission spectra of fluorescein (FITC, green) and R-phycoerythrin (PE, yellow), both excited by light from a blue (488 nm) laser (blue vertical line). Note that a portion of the FITC emission spectrum overlaps most of the PE emission spectrum.

Basic rules to minimize need for compensation

1. Match fluorophores to targets according to brightness needed (use the brightest dyes for least abundant or most disperse targets).
2. Consider the emission spectrum of the donor fluorophore when using tandem dyes. If possible, refrain from using tandem dyes if compensation minimization is the primary goal.
3. Know your instrument configuration—choose dyes that will work with the instrument's laser and filter configurations and, if spatially separated lasers are installed, maximize the use of lasers to minimize spillover.

But if you need to use compensation anyway...

1. Controls must be at least as bright as any samples to which compensation will be applied.
2. Background fluorescence at each wavelength should be the same for both the positive and negative control populations.
3. Use a tool such as the Molecular Probes™ Fluorescence SpectraViewer (thermofisher.com/spectraviewer) to determine the spillover of each dye in each detection channel (see page 22).

For example, by exciting FITC along the blue (488 nm) laser pathway and PE along the yellow (561 nm) laser pathway, the two fluorophores can be independently detected without the need for compensation (Figure 2). We have taken advantage of the Attune™ NxT cytometer's optical path layout to develop a no-lyse/no-wash, 6-color immunophenotyping panel to identify human T cell subsets without the need for compensation at any step (Figure 3). Find out more about the Attune™ NxT Acoustic Focusing Cytometer on page 19 and by visiting thermofisher.com/attunebp71. ■

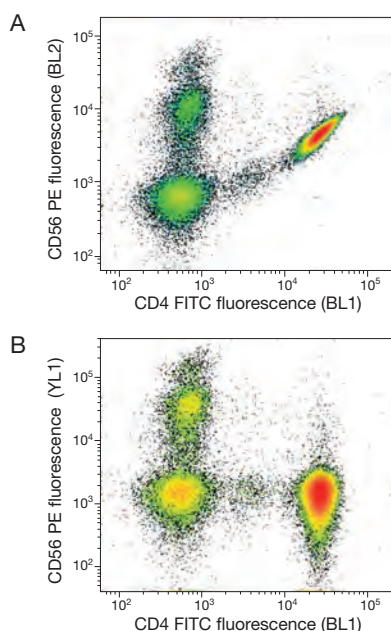


Figure 2. Elimination of FITC spillover into the PE channel using a yellow laser. When FITC and PE use the same optical detection pathways after excitation by the blue (488 nm) laser, there is significant spillover of FITC signal into the PE detector, requiring compensation. However, when excitation and detection paths of FITC and PE are uncoupled in the Attune™ NxT cytometer using the yellow (561 nm) laser to excite PE, there is little or no spillover of FITC signal into the PE detector; thus, no compensation is required. Data were acquired using **(A)** 488 nm excitation with a 530/30 nm bandpass (BP) filter to detect FITC and a 590/40 nm BP filter to detect PE, and **(B)** 488 nm excitation with a 530/30 nm BP filter to detect FITC, and 561 nm excitation with a 585/16 nm BP filter to detect PE.

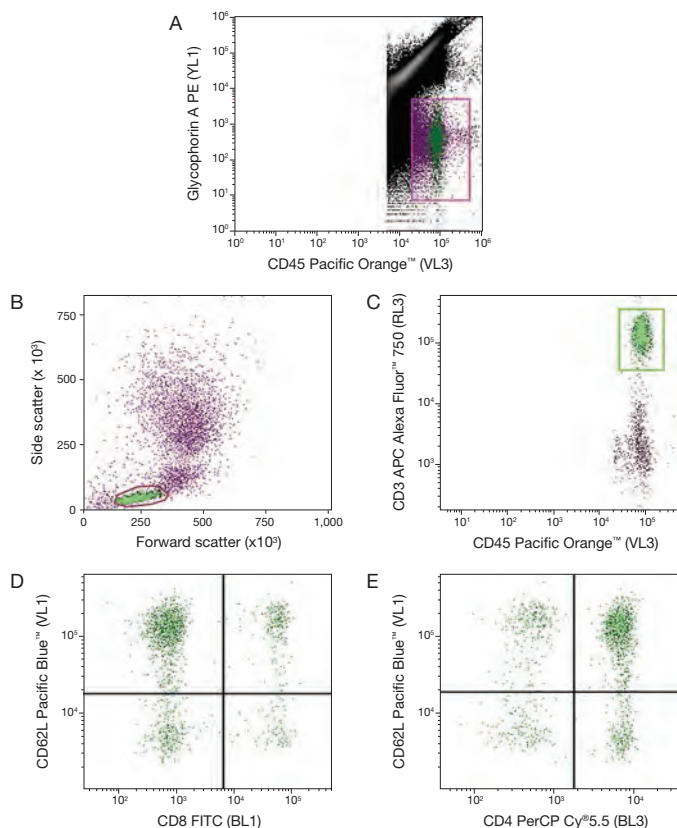


Figure 3. Optimal design of a no-lyse/no-wash, 6-color immunophenotyping panel for human T cell subsets acquired on the Attune™ NxT Acoustic Focusing Cytometer without using compensation at any step. Human whole blood was stained and interrogated using the probes and configurations described in Table 1. **(A)** A fluorescence threshold was set on Pacific Orange™ fluorescence (CD45), and events coincident with red blood cells were excluded based on PE positivity (glycophorin A or Gly A). **(B)** Lymphocytes were gated based on scatter properties, from which **(C)** T cells were identified by CD3 expression. **(D, E)** T cells were then analyzed for their expression of the lineage markers CD4 and CD8 as well as the activation marker CD62L in order to identify naive/central memory T cells (CD62L-positive) and effector memory T cells (CD62L-negative). No compensation was required to analyze or display these data.

Table 1. Lasers, filters, and probes for the no-lyse/no-wash, 6-color immunophenotyping panel acquired on the Attune™ NxT Acoustic Focusing Cytometer and shown in Figure 3.

Laser	Detection channel	Bandpass emission filter	Target	Antibody label	Antibody Cat. No.
Blue (488 nm)	BL1	530/30 nm	CD8	FITC	MHCD0801
	BL2				
	BL3	695/40 nm	CD4	PerCP-Cy5.5	A15858
Yellow (561 nm)	YL1	585/16 nm	Gly A	PE	MHGLA04
	YL2				
	YL3				
	YL4				
Violet (405 nm)	VL1	440/50 nm	CD62L	Pacific Blue™	MHCD0828
	VL2				
	VL3	603/48 nm	CD45	Pacific Orange™	MHCD4530
	VL4				
Red (637 nm)	RL1				
	RL2				
	RL3	780/60 nm	CD3	APC-Alexa Fluor™ 750	MHCD0327

First, do no harm

No-lyse, no-wash assays for the Attune™ NxT Acoustic Focusing Cytometer.

A key objective in many cell biology workflows is to maintain the cells' native characteristics throughout the analysis. Minimal sample preparation and manipulation helps to ensure that researchers are studying the natural state of the cell, and not an artifact of the enrichment or processing protocols. With its limited sample collection rates, however, a conventional hydrodynamic focusing cytometer restricts the volumes that can be analyzed in a timely and efficient manner, necessitating enrichment procedures that can result in phenotypic changes as well as loss of rare cell types [1].

In contrast, acoustic focusing cytometry allows high sample collection rates (up to 1,000 $\mu\text{L}/\text{min}$) without any loss in data resolution, thus reducing the need for pre-acquisition enrichment and allowing for detection of rare events in a heterogeneous population of cells. In addition, difficult-to-collect samples such as mouse blood and

bone marrow or thin-needle aspirates can be stained and diluted without washing or performing red blood cell lysis.

Benefits of acoustic focusing for analyzing rare-cell populations

In human whole blood, red blood cells outnumber leukocytes (white blood cells) by ~1,000 to 1. This imbalance creates two hurdles when attempting to analyze leukocytes in whole blood samples without manipulation: (1) collecting a sufficient number of leukocyte events to have statistically meaningful data, and (2) distinguishing leukocytes from red blood cells given the high probability of coincident red blood cell events. Figure 1A shows a conventional 488 nm side scatter (SSC) vs. forward scatter (FSC) profile of whole blood in which the two cell types cannot be resolved; Figure 1B shows improved resolution of the two cell types when violet 405 nm SSC is used.

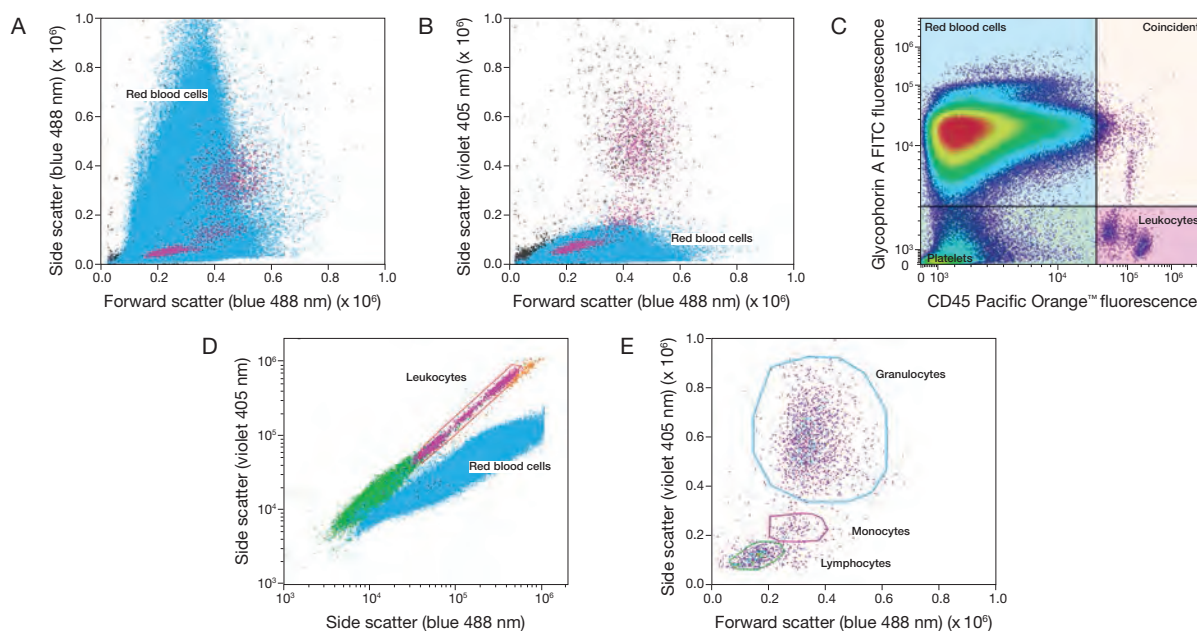


Figure 1. Identification of leukocytes in human whole blood using violet side scatter on the Attune™ NxT Acoustic Focusing Cytometer. (A) Using conventional blue 488 nm forward scatter (FSC) and side scatter (SSC) does not allow resolution of leukocytes in whole blood. Backgate analysis using fluorescently labeled antibodies specific for leukocytes (pink) and red blood cells (blue) demonstrates this problem. (B) Resolution of leukocytes from red blood cells in whole blood is improved by incorporating violet 405 nm SSC using the Attune™ NxT No-Wash No-Lyse Filter Kit (Cat. No. 100022776). (C) Backgate analysis using antibodies against the red blood cell marker glycophorin A (Cat. No. MHGLA014) and the leukocyte marker CD45 (Cat. No. MHCD4530TR) demonstrates the ease of identifying leukocytes in human whole blood, in contrast to the FSC and SSC analyses in (A) and (B). (D) Using both violet and blue SSC allows identification of leukocytes in whole blood, which is corroborated by the backgate analysis using glycophorin A and CD45 labeling depicted in (C), and demonstrates the different scatter properties of leukocytes and red blood cells when using violet SSC. (E) When leukocytes are gated based on violet light scatter properties, the three main leukocyte cell populations in human blood can be distinguished: lymphocytes, monocytes, and granulocytes.

Standard methods for isolating and detecting leukocytes in human whole blood are time consuming and often involve significant enrichment and manipulation prior to analysis. These sample preparation steps can result in alterations in cell physiology and loss of cell types of interest [1]. To overcome sample manipulation and enrichment artifacts and slow sample run times, we have developed three different no-lyse, no-wash protocols for identifying leukocytes in human whole blood on the Attune™ NxT Acoustic Focusing Cytometer, as well as a no-lyse, no-wash assay for phagocytic function.

Three no-lyse, no-wash protocols for leukocyte detection

The first leukocyte detection strategy exploits the difference in light-scattering properties between red blood cells and leukocytes. Red blood cells contain hemoglobin, a molecule that readily absorbs violet laser (405 nm) light, whereas leukocytes do not (Figure 1B), resulting in a unique scatter pattern for human whole blood with blue (488 nm) and violet (405 nm) SSC [2]. Inclusion of the Attune™ NxT No-Wash No-Lyse Filter Kit in the Attune™ NxT Acoustic Focusing Cytometer filter configuration allows simultaneous measurement of both blue and violet SSC and the differentiation of red blood cells and leukocytes based on light-scattering properties alone (Figure 1D), which we have validated using fluorescent antibodies that label CD45-expressing leukocytes or glycophorin A-expressing red blood cells (Figure 1C). The leukocytes can be further differentiated into granulocytes, monocytes, and lymphocytes by drawing a polygon gate around the leukocyte population and then plotting violet SSC vs. blue FSC (Figure 1E).

The next two no-lyse, no-wash strategies involve the use of fluorescent probes that are specific for markers expressed by red blood cells or leukocytes. For example, red blood cells express glycophorin A and leukocytes express CD45. Because the expression of these two markers is mutually exclusive, fluorophore-conjugated antibodies that recognize these two markers allow clear identification of red vs. white blood cells and exclusion of any red blood cell-coincident events (Figure 1C). Alternatively, the Vybrant™ DyeCycle™ dyes are cell-permeant nucleic acid stains that can be used to label nucleated cells. Because mature red blood cells are anucleate whereas leukocytes are nucleated, staining with one of the Vybrant™ DyeCycle™ dyes can distinguish red vs. white blood cells (Figure 2).

A no-lyse, no-wash assay for phagocytic function

We have also developed a no-lyse, no-wash functional assay using pHrodo™ *E. coli* BioParticles™ conjugate to assess phagocyte function in human whole blood using the Attune™ NxT cytometer. Phagocytic cells—such as neutrophils and monocytes—are key components of the innate immune system, serving as a critical line of defense against invading pathogens [3]. Monocytes mature into macrophages or inflammatory dendritic cells upon receiving various stimuli [4]. Characterizing the functional capacity of these phagocytic cell types in a whole blood no-lyse, no-wash assay saves time and reduces the potential artifacts that can be introduced during red blood cell lysis and multiple purification, centrifugation, and wash steps. Moreover, minimal sample processing and short acquisition times help keep cells healthy for multiplex functional assays.

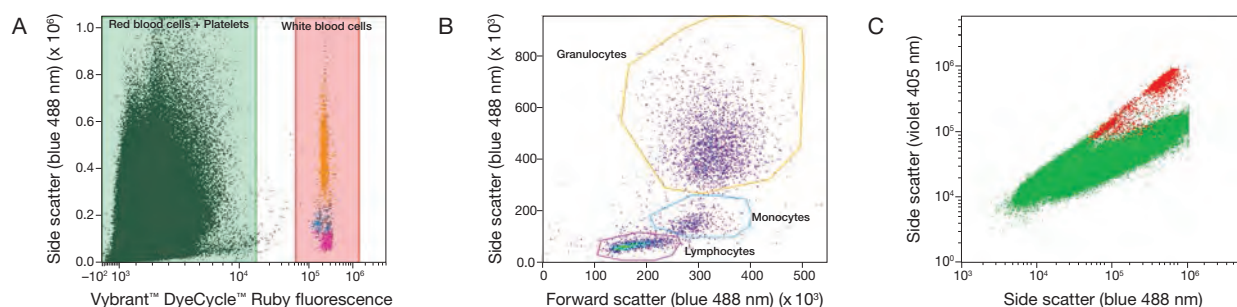


Figure 2. Identification of leukocytes in human whole blood using Vybrant™ DyeCycle™ dyes and the Attune™ NxT Acoustic Focusing Cytometer. The cell membrane-permeant Vybrant™ DyeCycle™ dyes label live nucleated cells, thus allowing identification of leukocytes in human whole blood. **(A)** Human whole blood was labeled with Vybrant™ DyeCycle™ Ruby Stain (Cat. No. V10309) to identify leukocytes by DNA staining. **(B)** Analysis of the blue forward scatter (FSC) and side scatter (SSC) properties of the Vybrant™ DyeCycle™ Ruby Stain-labeled cells discriminates the three main leukocyte populations in human blood: lymphocytes, monocytes, and granulocytes. **(C)** Use of the Attune™ NxT No-Wash No-Lyse Filter Kit (Cat. No. 100022776) with violet differential scatter confirms the ability of Vybrant™ DyeCycle™ Ruby Stain to identify leukocytes in a whole blood sample.

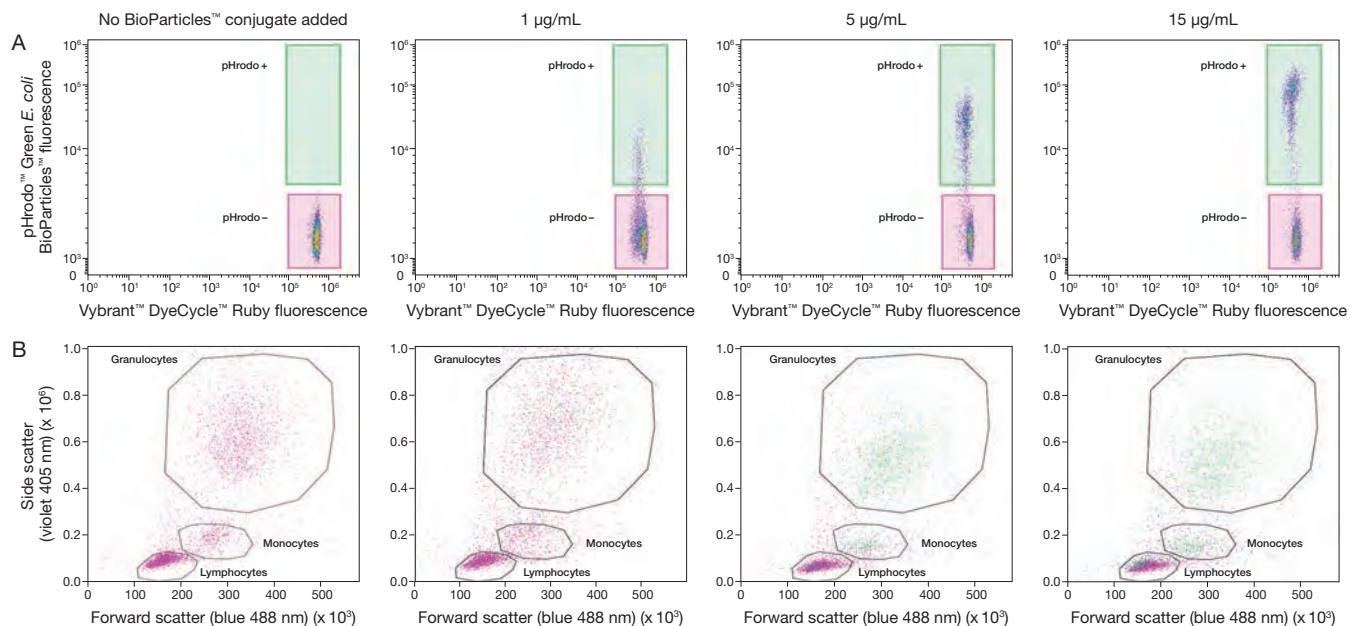


Figure 3. Dose-response plots for pHrodo™ Green *E. coli* BioParticles™ conjugate show multiple phagocytic cell types in a human whole blood no-lyse, no-wash assay. Whole blood was incubated with 1, 5, or 15 µg/mL pHrodo™ Green *E. coli* BioParticles™ Conjugate [Cat. No. P35366] or left untreated for 30 min at 37°C and 5% CO₂, diluted, and then labeled with Vybrant™ DyeCycle™ Ruby Stain for 15 min at 37°C and 5% CO₂. **(A)** As the concentration of pHrodo™ Green BioParticles™ conjugate increases, the frequency of phagocytic cells that are positive for pHrodo™ dye increases along with a shift in green-fluorescent mean fluorescence intensity (MFI) at the higher concentrations of pHrodo™ Green BioParticles™ conjugate. **(B)** At 15 µg/mL pHrodo™ Green BioParticles™ conjugate, it is evident that there are subpopulations within the granulocyte, monocyte, and lymphocyte gates that have actively phagocytosed the pHrodo™ conjugate (green data points).

In our no-lyse, no-wash phagocytic assay, we incubated whole blood with pHrodo™ Green *E. coli* BioParticles™ conjugate for 15 to 30 min, and then labeled cells with Vybrant™ DyeCycle™ Ruby Stain, a cell-permeant nucleic acid dye. pHrodo™ BioParticles™ conjugates are killed bacteria (*E. coli* or *S. aureus*) or yeast zymosan (from *S. cerevisiae*) labeled with pHrodo™ dyes—pH sensors that are nonfluorescent at neutral pH and exhibit increasing fluorescence as pH becomes more acidic. Phagocytic cells that have internalized the pHrodo™ Green or pHrodo™ Red BioParticles™ conjugates into phagosomes (pH ~5) fluoresce green or red, respectively, and this internalization is inhibited at 4°C.

Figure 3A shows that as the concentration of pHrodo™ BioParticles™ conjugate increases, the frequency of phagocytic cells that are positive for pHrodo™ dye increases. Furthermore, the dose-response data coupled with violet SSC vs. blue FSC gating shows the three major leukocyte subpopulations—granulocytes, monocytes, and lymphocytes (Figure 3B). At concentrations of ≤5 µg/mL pHrodo™ BioParticles™ conjugate, neutrophils (within the granulocyte population) and monocytes appear to be the primary phagocytic cell types. As the concentration of pHrodo™ BioParticles™ conjugate increases, greater frequencies of neutrophils and

monocytes show a positive pHrodo™ signal, as does a population within the standard lymphocyte gate, which are likely dendritic cells.

Multiplexing with the Attune™ cytometer

With the 4-laser, 16-detection channel Attune™ NxT Acoustic Focusing Cytometer, these no-lyse, no-wash assays can be multiplexed with Molecular Probes™ reagents to identify specific cell types as well as changes in cell function. Learn about applications for the Attune™ NxT cytometer at thermofisher.com/attuneappnotesbp71. ■

References

1. Gratama JW, Menendez P, Kraan J et al. (2000) *J Immunol Methods* 239:13–23.
2. Ost V, Neukammer V, Rinneberg H (1998) *Cytometry* 32:191–197.
3. Segal AW (2005) *Annu Rev Immunol* 23:197–223.
4. Tacke F, Randolph GJ (2006) *Immunobiology* 211:609–618.

Product	Quantity	Cat. No.
pHrodo™ Green <i>E. coli</i> BioParticles™ Conjugate	5 x 2 mg	P35366
pHrodo™ Green <i>E. coli</i> BioParticles™ Phagocytosis Kit	1 kit	P35381
pHrodo™ Green <i>S. aureus</i> BioParticles™ Phagocytosis Kit	1 kit	P35382
pHrodo™ Red <i>E. coli</i> BioParticles™ Phagocytosis Kit	1 kit	A10025
Vybrant™ DyeCycle™ Green Stain	400 µL	V35004
Vybrant™ DyeCycle™ Orange Stain	400 µL	V35005
Vybrant™ DyeCycle™ Ruby Stain	100 assays	V10309
Vybrant™ DyeCycle™ Violet Stain	200 µL	V35003

RECENTLY PUBLISHED



Multiparameter detection of early apoptosis markers without compensation

Uncompensated polychromatic analysis of mitochondrial membrane potential using JC-1 and multilaser excitation.

De Biasi S, Gibellini L, Cossarizza A (2015) *Curr Protoc Cytom* 7.32.1–7.32.11.

Disruption of the mitochondrial membrane potential has been shown to accompany cell stress and early apoptosis. De Biasi and coworkers recently described a new version of their original flow cytometry protocol to measure mitochondrial membrane potential using the lipophilic cation JC-1. The JC-1

dye reversibly accumulates in mitochondrial membranes in a potential-dependent manner: at low membrane potential, JC-1 exhibits green fluorescence (~530 nm) and exists as a monomer; at higher potential, it forms red-fluorescent (~590 nm) "J-aggregates" in the mitochondrial membrane. The ratio of green to red fluorescence emission of JC-1 is thus proportional to the degree of mitochondrial membrane depolarization. Because early apoptotic cells exhibit disrupted mitochondrial membrane potential, JC-1 can be used as an early marker of apoptosis, alone or in combination with other apoptosis probes.

In the authors' original JC-1 detection protocol, a flow cytometer equipped with only a single 488 nm (blue) laser was used for the analysis, requiring compensation between the two detection channels for JC-1 monomer and J-aggregate emission. The updated method described in this article employs the Attune™ NxT Acoustic Focusing Cytometer, an instrument available with up to four lasers (blue, red, violet, and yellow lasers). The use of multiple lasers for excitation minimizes the need for compensation, allowing for a simpler and more efficient detection protocol. Multilaser excitation also permitted the authors to develop a second protocol for the simultaneous detection of mitochondrial membrane potential changes and additional apoptosis markers, including the externalization of phosphatidylserine and the formation of reactive oxygen species.

The updated JC-1 detection protocol described by De Biasi et al. makes use of two lasers for JC-1 detection: the blue (488 nm) laser to excite JC-1 monomers and the yellow (561 nm) laser to excite J-aggregates. As shown in Figure 1, U937 cells were treated with valinomycin, a K⁺ ionophore that depolarizes the mitochondrial membrane, and then stained with JC-1. The treated cells are shifted to the bottom-right of the plot, →

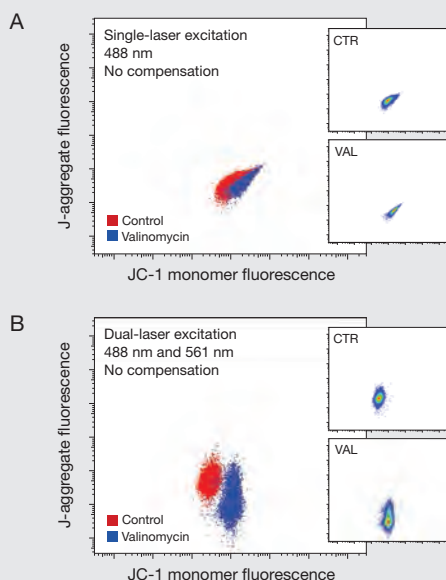


Figure 1. Uncompensated multilaser analysis of JC-1 fluorescence after mitochondrial membrane depolarization in U937 cells. Control U937 (human leukemic monocyte lymphoma) cells (CTR) were stained with 2.5 µg/mL JC-1; experimental U937 cells were treated with 1 µM valinomycin (VAL) for 15 min to depolarize mitochondria prior to JC-1 staining. Samples were acquired without compensation on the Attune™ NxT cytometer using (A) only a 488 nm laser for excitation and 530/30 nm and 574/26 nm bandpass (BP) filters for detection of JC-1 monomers and J-aggregates, respectively; or (B) both the 488 nm and 561 nm lasers for excitation and 530/30 nm and 585/16 nm BP filters for detection of JC-1 monomers and J-aggregates, respectively. Small insets show individual CTR and VAL plots; large plots show merged CTR and VAL data in order to visualize the JC-1 monomer and J-aggregate signals together. Data provided by Sara De Biasi, Lara Gibellini, and Andrea Cossarizza, University of Modena and Reggio Emilia, Italy.

representing an increase in JC-1 monomers. When single-laser excitation is used without any compensation, the J-aggregate and JC-1 monomer emissions cannot be easily separated in the plot of red vs. green fluorescence (Figure 1A); with dual-laser excitation, however, no compensation is required to distinguish the fluorescence emission of the two forms of JC-1 (Figure 1B).

For simultaneous detection of multiple markers of apoptosis, the authors used two additional probes: Pacific Blue™ annexin V (to detect exposed phosphatidylserine residues with the violet laser) and CellROX™ Deep Red Reagent (to detect reactive oxygen species with the red laser). Using four lasers simultaneously on the Attune™ NxT cytometer without compensation, they demonstrated the detection of all three apoptosis markers

(Figure 2). They suggest that these protocols can be adapted for multiparameter detection of apoptosis using a variety of fluorescent cell function probes. ■

Product	Quantity	Cat. No.
Annexin V, Pacific Blue™ conjugate, for flow cytometry	500 µL	A35122
Attune™ NxT Acoustic Focusing Cytometer—Blue/Yellow Lasers	1 each	A24861
Attune™ NxT Acoustic Focusing Cytometer—Blue/Red/Violet/Yellow Lasers	1 each	A24858
CellROX™ Deep Red Reagent, for oxidative stress detection	5 x 50 µL	C10422
CellROX™ Deep Red Flow Cytometry Assay Kit	100 assays	C10491
JC-1 Dye (Mitochondrial Membrane Potential Probe)	5 mg	T3168
MitoProbe™ JC-1 Assay Kit	1 kit	M34152

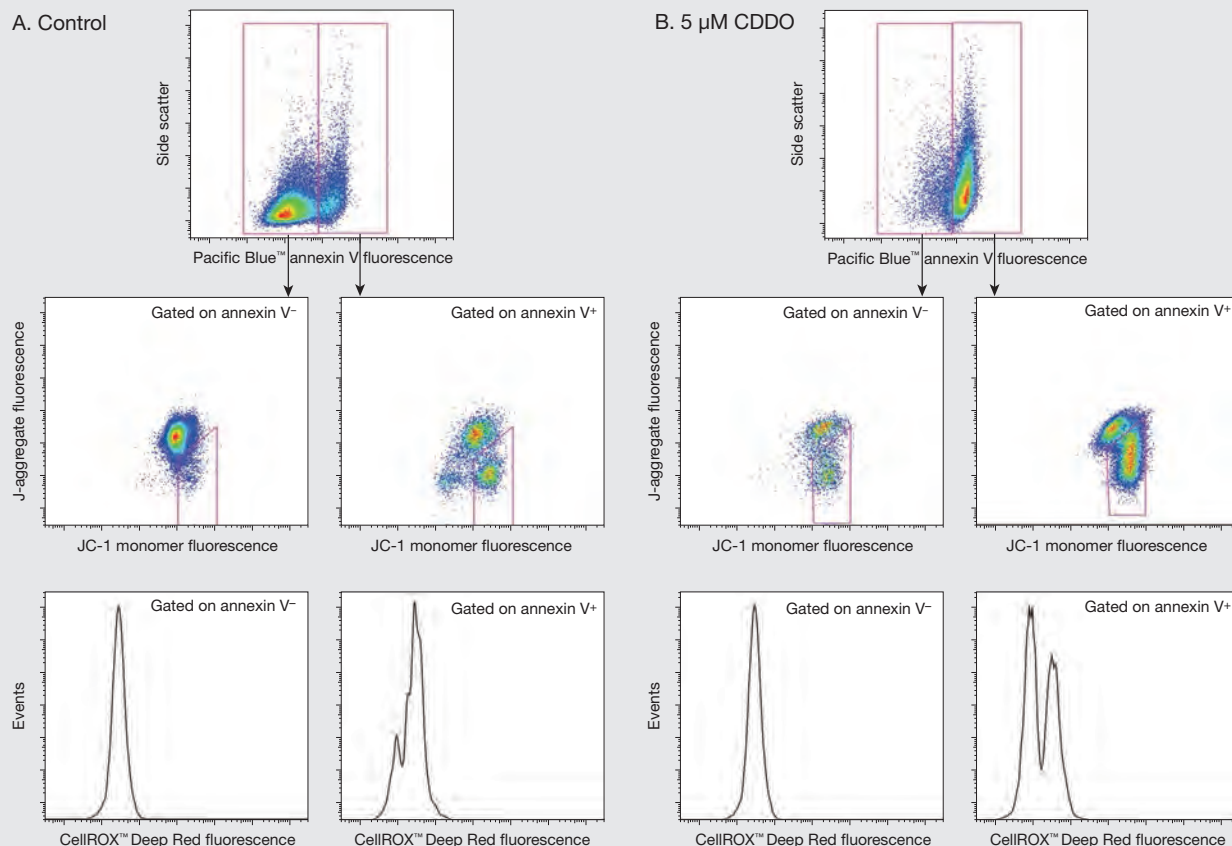


Figure 2. Uncompensated multilaser analysis of apoptosis, mitochondrial membrane potential, and reactive oxygen species (ROS) production in RKO cells. RKO colon cancer cells were cultured for 24 hr in the (A) absence or (B) presence of 5 µM CDDO (2-cyano-3,12-dioxo-oleana-1,9(11)-dien-28-oic acid, methyl ester), a Nrf2 activator that can inhibit cell proliferation and induce differentiation and apoptosis. Cells were stained with Pacific Blue™ annexin V, JC-1, and CellROX™ Deep Red Reagent, and data were collected using the 4-laser Attune™ NxT Acoustic Focusing Cytometer without compensation. Viable and apoptotic cells were identified by negative and positive Pacific Blue™ annexin V staining, respectively (405 nm laser, 440/50 nm BP filter); mitochondrial membrane potential was analyzed with JC-1 (488 nm and 561 nm lasers with filters described in Figure 1); reactive oxygen species (ROS) production was detected using CellROX™ Deep Red Reagent (637 nm laser, 670/40 nm BP filter). Reprinted from De Biasi S, Gibellini L, Cossarizza A (2015) *Curr Protoc Cytom* 7.32.1–7.32.11, with permission from *Current Protocols in Cytometry*.